Growth of hexagonal SiGe nanowire branches

Kaman, Wouter H.

Award date:
2018

Growth of hexagonal SiGe nanowire branches

Wouter Kaman

2017-2018

Supervisors:
Yizhen Ren M.Sc[1]
prof. dr. Erik P.A.M Bakkers[1]

[1]: Advanced nanomaterials and devices, Department of Applied Physics, Eindhoven University of Technology (AND,TU/e), Eindhoven, The Netherlands

Abstract

Nowadays almost all electronic devices include integrated circuits made from silicon. Although silicon is cheap and relatively easy to make compared to other semiconductors, it has its limits. Processing clock speeds haven't gone up since 2004 due to the lack of thermal management. One solution to this problem is optoelectronics in which a SiGe laser is used to transfer data. Silicon and germanium both crystallize in the cubic crystal phase which exhibits an indirect bandgap. However, theoretical calculations show that an alloy of silicon and germanium in the hexagonal crystal phase will have a direct bandgap. To fabricate hexagonal silicon, a wurtzite GaP nanowire is grown by using metal-organic vapor phase epitaxy, with a silicon shell around the GaP core. This silicon shell copies the hexagonal crystal structure of the of the GaP nanowire, creating hexagonal silicon. One way to omit the GaP core is by growing horizontal SiGe branches on a hexagonal (core-)shell nanowire. These branches copy the hexagonal crystal structure and thus make pure hexagonal SiGe material, which can then potentially be made into a laser.

In this work the growth and optimization of hexagonal SiGe is described. Different precursors, substrates, growth temperatures and flows are studied. The optimal straight Si branches are grown with disilane, on a Si shell, at a temperature of 650°C and with a flow of 0.35Ssccm. In this work it is proven that it is possible to grow hexagonal silicon branches with very few defects. The germanium branches gold catalyst regime is between 430-470°C. Due to the different growth regimes, growing heterostructures and incorporating germanium in silicon branches for direct bandgap material opposed a great challenge. The number of kinks per micron was minimized at a flow 0.35 sccm, at which the gold droplet preserves the most stable contact angle with the nanowire interface. The kinking angle is predominantly 120° with fewer 60° angles, caused by nucleation happening at the active {11-20} facet of the three-face boundary. This causes one or two triangular joints connecting the two arms in the <10-10> direction. Cross-section TEM images of the branches showed a hexagonal shape, which is in contrast to earlier measurements found in literature.

Index

1 Introduction

Nowadays almost all electronic devices include integrated circuits made from silicon as their main source of computation power. Due to the fact that silicon is a semiconductor and can be manufactured in a high crystal quality at a low price point, it is ideal to use as a material for producing integrated circuits, especially compared to other semiconductors used in the industry. Silicon is after oxygen the second most abundant element in the world, which is around 28% of the mass of the earth crust.[1] Although silicon is almost never found in a pure state, but more commonly found as silica (SiO_2) and other silicates. It can be extracted from sand as silica in a rough and highly contaminated form easy.[2] Silica can be made into an amorphous, polycrystalline and a mono-crystalline crystal phase, of which the latter is used in the production of integrated circuits. The natural mono-crystalline form of silicon is the diamond cubic crystal structure. The reason why a mono-crystalline crystal phase is needed, is because grain boundaries in the lattice and other discontinuities would influence the properties of the material negatively.[3]

Although silicon has proven itself as being highly reliable material for integrated circuits, silicon also has its limits. When comparing the processing chips produced at the moment to the processors produced after 2004. The clock speed hasn't gone up significantly. The limiting factor is the power needed to transport all the information, at these high frequencies. A higher clock speed means that there is more current passing through and in between transistors generating more heat. This excess heat cannot be cooled quick enough and therefore it is not efficient to increase the processor speed due to the amount of energy wasted on cooling the chip. One solution to this problem is making use of optoelectronics.

Optoelectronics is the combination of optics and electronics to source, detect and control electronically generated data into light emission as means of data transportation. One way to convert an electronic signal into light is by fabricating of a laser. The laser can be electrically pumped giving a light signal, which can then be used a signal to transfer data. To emit light, a semiconductor requires a direct band gap. Silicon crystalizes in the cubic crystal phase, which has an indirect band gap. Other semiconductors such GaAs and InAs, which can also be used as a material for integrated circuits do have direct bandgap, but since the entire chip industry is nowadays build around silicon and silicon is a lot cheaper, there is legitimate incentive to investigate a solution to make silicon lase.

One solution in creating a direct bandgap for silicon was already discovered in 1973. It was predicted with tight-binding calculations that silicon gets an almost direct bandgap when its crystal lattice is hexagonal.[4,5] By alloying silicon with germanium content higher than 65% in a hexagonal crystal structure, the top of the valence band and the minima of the conduction band at the Γ-point would lie above each other, creating a direct band gap. By changing the crystal structure of SiGe a laser can be fabricated. Although the theory is promising, fabricating hexagonal silicon and germanium in large stable domains hasn't been realized yet. Several attempts have been tried, e.g. hexagonal silicon formation by pulsed laser beam annealing[6], temperature annealing by exerting lateral outward stress in nanowires creating hexagonal nano-ribbons[7] and hexagonal silicon grain formation as side effect during the deposition of SiO_2 films.[8]

To make larger stable hexagonal silicon domains, one solution is making use of core-shell nanowires. Due to their large aspect ratio, nanowires have the ability to relieve the mismatch strain laterally over a short distance from the interface.[9,10] Nanowires are an ideal candidate for combining mismatched materials while preserving a high crystal quality, such as core-shell nanowires.[11] By first growing a wurtzite GaP core and then epitaxially grown a silicon shell around the core, the hexagonal (wurtzite) crystal structure of the core will be copied into the shell, resulting in hexagonal silicon. The fabrication of a wurtzite GaP and a low defected Si shell has been presented by earlier members of the group.[12] A cross-sectional energy-dispersive X-ray (EDX) map of these core-shell nanowires can be seen in *figure 1.1a* and a top-view in *figure 1.1b*. The good epitaxial relationship between the GaP core and the Si shell is shown in *figure 1.2b*. These same core-shell nanowires are also used in this work.

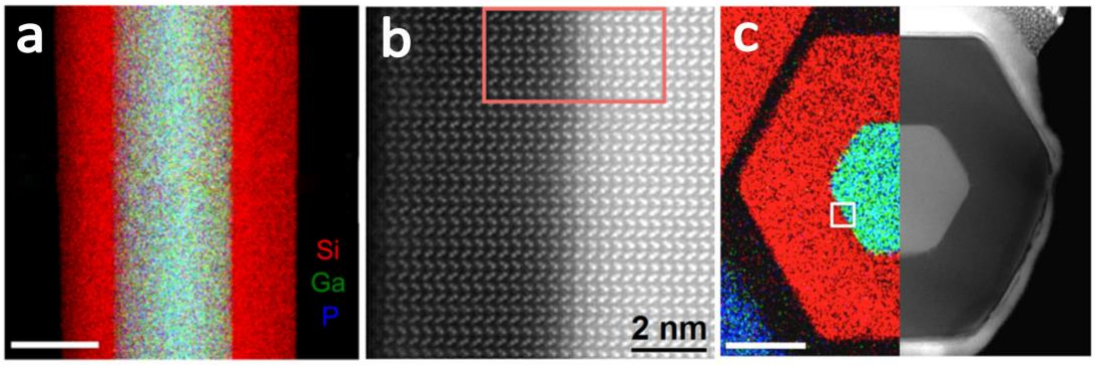

Figure 1.1 – (a) shows an EDX mapping of a GaP core with Si shell nanowire. The elements are color-coded red for silicon, green for gallium and blue for phosphor. (b) A high-resolution scanning transmission electron microscopy (HR-STEM) image at the GaP core/Si shell interface, with a good epitaxial relationship copying the crystal structure from the core into the shell. (c) A top-view EDX map (left) and high-angle annular dark-field scanning transmission electron microscopy (HAADF-STEM) image (right) taken in the [0001] direction. The white scale bars represent 100nm. Images edited – Hauge et al[12].

The disadvantage of core-shell nanowires (NWs) is that the gain medium is not purely hexagonal SiGe, but there are always GaP core present. In this project a solution to omit the GaP core is investigated by growing branched nanowires. By depositing Au particles on the sidewalls of the hexagonal NWs, branches can be grown by the vapor-liquid-sold growth mechanism horizontally on the core-shell nanowire. The crystal structure will be extended into the branches resulting in a pure hexagonal material without the need of a core as a template. These structures resemble branches growing out of a tree trunk. A branch could thus have more gain material compared to a core-shell nanowire with the same dimensions. The purity of the gain medium can be increased when using branches. Since Ga and P atoms are dopants for group IV semiconductors this will affect the optical properties. By separating the growth from these dopants there is no contamination coming from the core. The branch can also be grown in a p-i-n junction axially. The branch can then be contacted to be pumped electrically to make a laser. These branches can also be used as a proof of principle that pure hexagonal material can be grown in the form of a nanowire. With the origin of the crystal structure not arising from a defective cubic crystal lattice with induced strain and twining.[11,13]

All the studies performed on branched nanowires in recent years were performed on other systems than hexagonal SiGe. Examples are: growing branched GaP nanowires

in both a wurtzite and zincblende crystal phase[14], height controlling GaP nanowire branches[15] and silicon branched nanowire structures which exhibit a cubic crystal structure.[16] Hexagonal SiGe branches have also been grown on GaP cores.[17] Although these branches have proven that it is possible to grow pure hexagonal SiGe branches by coping the crystal structure of the core. The growth kinetics and parameters influencing the branch growth have not been not been studied. The width of the branches is small with a diameter of around 20nm. In *figure 1.2* a SEM images is shown of a hexagonal SiGe branches on bare GaP.

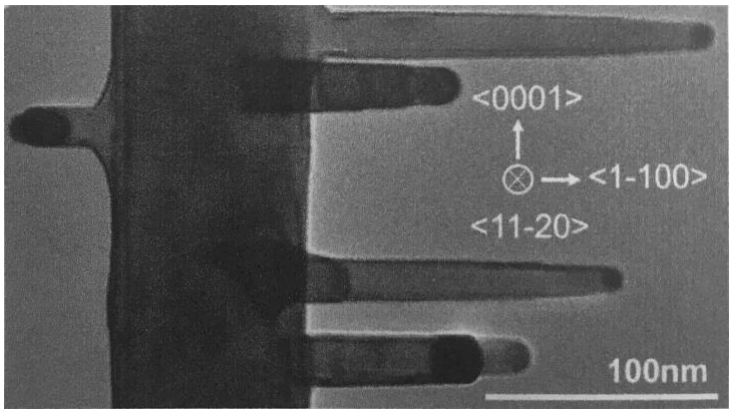

Figure 1.2 – Hexagonal SiGe branches on bare GaP. The branches are in the order of 20nm thick. Image taken - Hauge.[17]

In this work we want to investigate which parameters play an important role in the growth kinetics of SiGe branches. The branches are optimized to grow as wide and long as possible, for the potential application as a gain medium for a laser. Other growth properties such as kinking, kinking angle and point of nucleation of the branches is investigated. To get a direct bandgap material, germanium is incorporated in silicon branches via the silicon approach. And finally, SiGe heterostructures are tried to be grown by combining all data gained in prior experiments.

2 Theory

In this chapter the theoretical background of branches will be discussed, as well as theoretical insights which lead to important decisions made during this project. First the crystal structure and the theory behind hexagonal Si/Ge band gaps will be described. Then a general introduction on the fundamentals of nanowire growth will be given. A general overview will be given for the parameters influencing nanowire growth and how this will affect the grown branches. Then theory found in literature will be given for the kinking process and the kinking angle, which is used during the course of the project in studying the growth kinetics of the SiGe branched nanowires.

2.1 Crystal structure

In this work the crystal structure of the branched nanowires is of major importance, since it determines its optical and electric properties. A crystal structure is defined by its periodicity of atoms, ions or molecules which together form a regular lattice. By defining a unit cell in which all the geometric characteristics, symmetries and the base of the atoms is described. The entire lattice can then be described by repeating the unit cell in the lengths of the principal axes by simple vector additions. In this thesis we will mainly focus on two different types of lattices. The first one is the diamond cubic crystal structure. Which in our case can also be the zincblende crystal structure when two different species are present in the crystal lattice. The cubic diamond crystal structure is defined by a repeating pattern of 8 atoms who can be viewed as a pair of face-centered lattices, as shown in *figure 2.1a*. In the zincblende cubic lattice, the two atom types form two interpenetrating face-centered lattices. This means that the zincblende crystal structure is thus defined by having the four nearest neighbor atoms of the opposite type, like shown in *figure 2.1c*. In this work we have alternating gallium and phosphorous atoms. When looking into the [110] direction of the crystal lattices the ABCABC stacking of the cubic phase becomes visible.

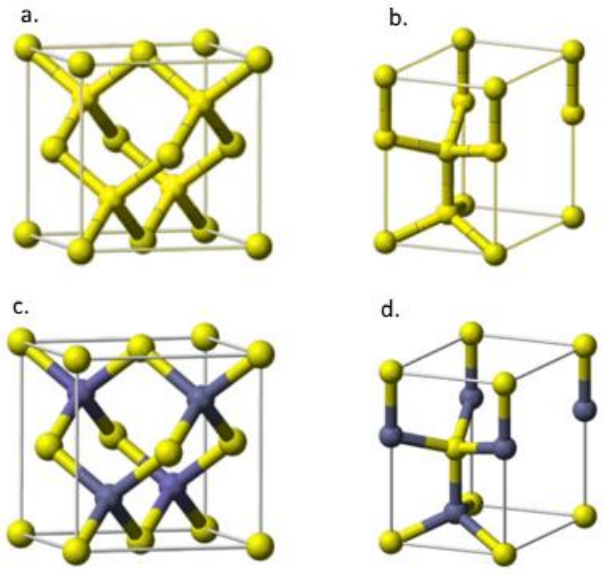

Figure 2.1 – The unit cells of the (a) diamond cubic crystal structure, (b) the hexagonal diamond, (c) the zincblende and (d) the wurtzite crystal structure. Both (a) and (b) as well as (c) and (d) are structurally the same but differ for the reason that (a) and (b) are occupied by the same species of atoms on all lattice sites, while in (c) and (d) each sub lattice is occupied by two different types of atoms. Image edited – crystallography365

The second crystal structure is the hexagonal diamond lattice. This lattice is a combination of two interpenetrating hexagonal close-packed (HCP) sub-lattices. The unit cell of the hexagonal diamond lattice can be seen in *figure 2.1b*. When two individual atoms form a sublattice which is HCP-type, then the hexagonal diamond lattice has a wurtzite structure as can be seen in *figure2.1d.* When looking in the [11-20] direction the ABABAB… stacking of the wurtzite stacking is visible as can be seen in *figure 2.2b*. Under the TEM this is visible as repeating "dumbbells". The ABCAB stacking of zinc blende is shown in *figure 2.2a.*

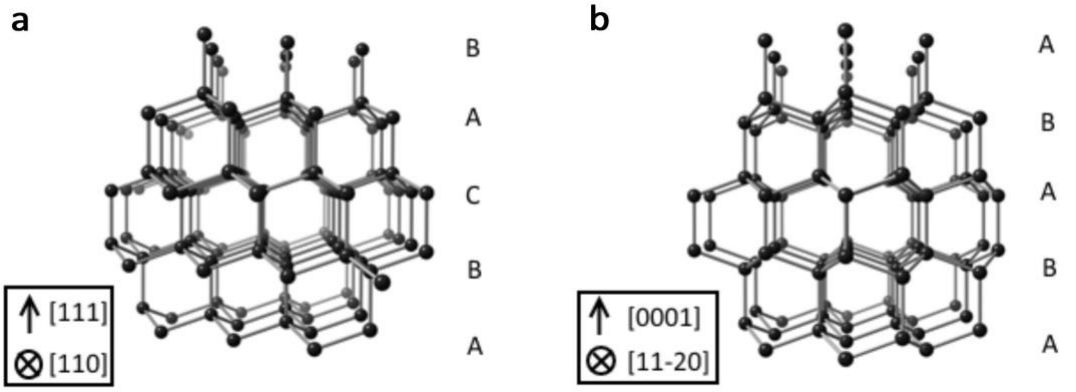

Figure 2.2 – A representation of the diamond cubic (a) and hexagonal crystal structure (b). (a) The diamond crystal is viewed along the [110] zone axis in which the ABCABC stacking becomes visible. (b) The hexagonal crystal structure viewed along the [11-2] zone axis in which the ABABAB stacking is visible. In the cubic crystal structure every 4th mono layer is precisely above the first monolayer. In the hexagonal crystal structure every 3th monolayer is precisely above the first monolayer. Image edited - Hauge.[17]

2.1.1 Brillouin zone of ZB and WZ crystals

In solid state physics the first Brillouin zone (BZ) is a uniquely defined primitive cell in reciprocal space. The importance of the Brillouin zone originates from the theory that the solution to Bloch's wave description in a periodic medium, can completely characterize its lattice behavior in a single Brillouin zone. Due to the periodicity of the lattice, deriving the band structure from a single BZ, essentially gives the full information about the band structure of the entire lattice. The center of the BZ is named the Γ-point, as can be seen in *figure 2.3.* This is true for both a diamond cubic crystal structure and the hexagonal diamond crystal structure. Together with other high symmetry points a band structure can be calculated, moving from one symmetry point to another. For the diamond cubic crystal structure, the most important symmetry points are the X-, K-, L points, which lie on the {100}, {110} and {100} surfaces of the Brillouin zone respectively. For the diamond cubic crystal structure, the most important high symmetry points are A- and M- points, which lie on the {0001} and {1-100} of the Brillouin zone respectively.[17]

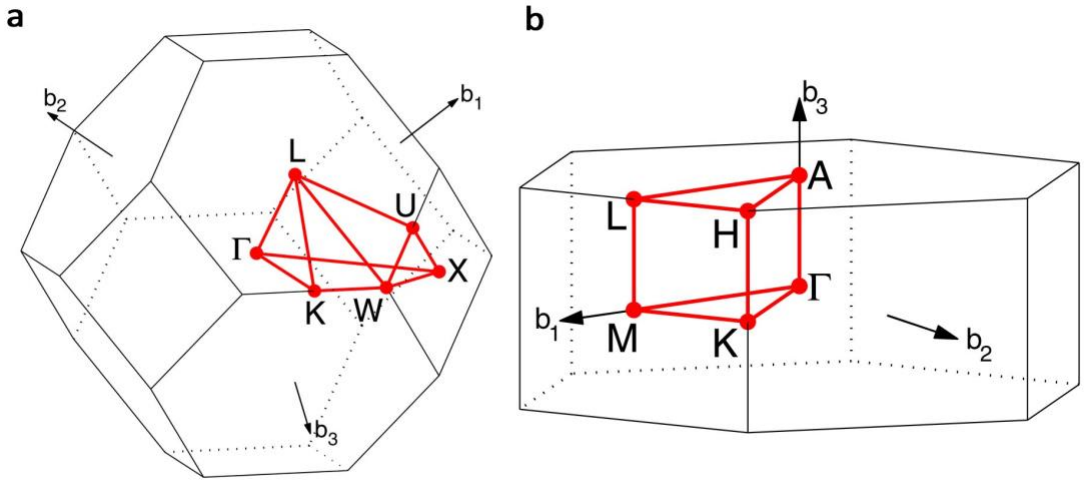

Figure 2.3 – First Brillouin zone of the diamond cubic crystal structure (a) and the first Brillouin zone of the hexagonal diamond crystal structure. For both the Brillouin zones the gamma point lies at the center. Image taken – wikiwand.com[18]

The cubic diamond structure has two atoms in its unit cell, while the hexagonal diamond crystal structure has four. This gives 2:1 mapping ratio between the between the BZ of the diamond cubic and the hexagonal crystal structure. Due to this phenomena some high symmetry points have overlapping known as folding.[19] Which implies that two points of the diamond cubic BZ are folded to one point of the hexagonal diamond BZ.[20] In this case the Γ- and L- point of the cubic BZ are folded onto the Γ-point of the hexagonal BZ. This can happen due to the fact that the BZ of the hexagonal crystal structure is much smaller. In this way the bandgap at the Γ-point of the hexagonal crystal structure can be estimated from the cubic Γ- and L- point. This could imply that the diamond cubic material with a conduction band minimum at the L-point could have a direct band gap in its hexagonal diamond polytype.[17]

2.1.2 Lattice mismatch, stacking faults and cracks

We have now defined the crystal structure, the unit cell and the Brillouin zone of cubic and hexagonal silicon or germanium. But what happens to the properties of the system when strain and defects are present in the lattice? Strain, cracks and stacking faults can have a negative effect on optoelectronic applications. They can degrade the electric transport properties by playing a role as recombination center and introducing trap states which significantly decrease the PL emission.[21] Although nanowires have effective strain relaxation due to their geometry, still defects like stacking faults can occur within the nanowire. Core-shell heterostructures are much more sensitive to strain than the axial heterostructure nanowires. The formation of misfit dislocation depends heavily on the strain of the core-shell nanowire due to lattice mismatch and the relative dimensions of the core and the shell. The lattice mismatch in the system can be calculated by using *equation 1 (see top of next page)*. in which a_1 is the lattice constant for species one and a_2 the lattice constant for species two. When comparing Zinc Blende GaP and Si we see that the lattice mismatch between zinc blende GaP and diamond Silicon is around 0,36%. Which is relatively small. This would be much larger when combining e.g. GaP and Ge as can be seen in *figure 2.4*. The lattice parameters for hexagonal silicon and wurtzite GaP are a = 3.82 Å, c=10.24 Å and a=3.842 Å, c= 6.335 Å respectively.[6,22]

$$L_{mismatch} = \frac{a_1 - a_2}{a_1}\, x\, 100 = \frac{5{,}45A - 5{,}43A}{5{,}45A} x\, 100 = \ 0{,}36\% \qquad (1)$$

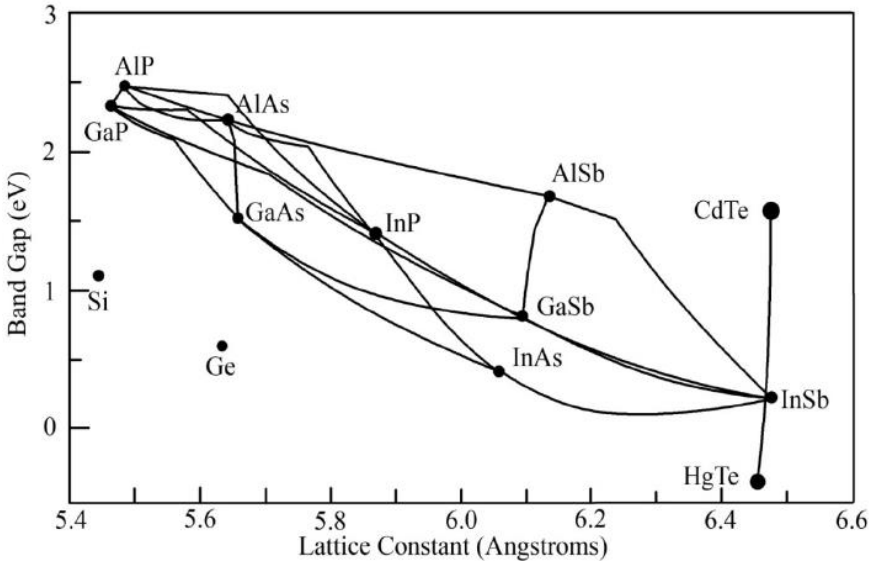

Figure 2.4 – The energy gap plotted versus the lattice constant. GaP and Si show around the same lattice constant with only a difference of 0,36%. GaAs and Ge show around the same lattice constant. This makes it difficult to grow epitaxially Ge branches on a GaP stem or growing radial heterostructure branches. Image taken – researchgate.net[23]

When a stacking fault is present in a zinc blende crystal lattice it can switch e.g. from ABCABC to ABABCABC, in this case crating a wurtzite monolayer. When a stacking fault occurs the order of stacking is reversed. Another defect is the presence of cracks. These cracks originate from the presence of a fractures in the Si shell surface. This defect thus does not seem to arise from an alteration of the stacking sequence of the lattice planes in the Si shell.[24] In the core-shell nanowires used in the project, cracks are present in the Si shell. Therefore, great caution has to be taken in studying these defects and their influence with respect to the crystal quality of the branches.

2.2 Band structure of Hexagonal Silicon-Germanium and light emission

In this project branched nanowires are studied to produce pure hexagonal material which could eventually lead to the production of a silicon-germanium laser. By looking at the high symmetry points in the BZ it is possible to construct a band diagram in reciprocal space of cubic Si and Ge. The bandgap is the energy difference between the valence band and the conduction band where no electron states can exist. A distinction is made between a direct and indirect bandgap. A direct bandgap allows an electron at the bottom of the conduction band to recombine with a hole at the top of the valence band. When both the hole at the top of the valence band and the electron at the bottom of the conduction band recombine, a photon is emitted during radiative recombination which is equal to the energy of the bandgap. In an indirect bandgap material, the top of the valence band and the bottom of the conduction band do not lie directly above one and other. Therefore, the emission or absorption of a phonon is needed to conserve the crystal momentum. This requires an extra quasi-particle to coincide with the electron and the hole creating a lower probability of this process occurring.[25] Due to this phenomena radiative combination and thus PL is more likely in a direct bandgap semiconducting material than an indirect bandgap semiconducting material.

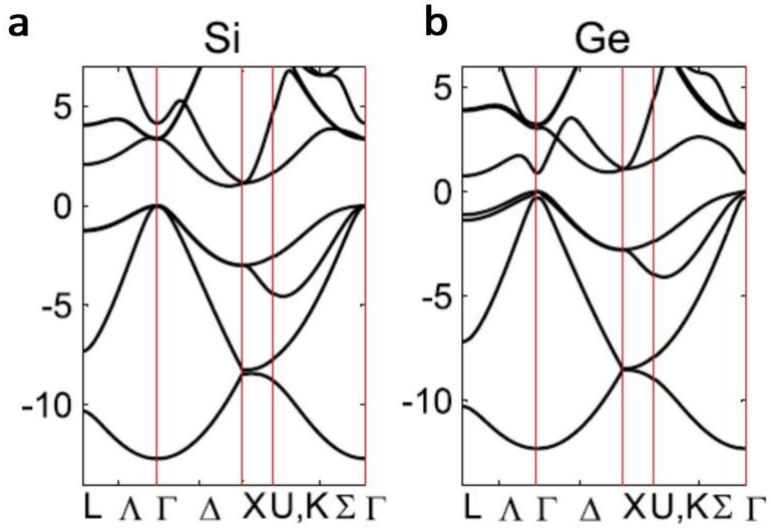

Figure 2.5 – The calculated band structures including spin-orbit coupling interactions for the cubic crystal phase of silicon (a) and germanium (b). Both the Si and Ge band diagram show an indirect bandgap, which makes them optically inactive. Image taken – De et al.[5]

When calculating the band structure including spin-orbit interactions of cubic Si and Ge, one can see that both materials are having an indirect bandgap and are therefore optically inactive. This can be seen in *figure 2.5*, in which both systems have their maxima of the valence band at the Γ-point and the bottom of the conduction band at the X- and L- point for Si and Ge respectively. When calculating the band structure of the hexagonal Si and the Ge crystal phase the band structures for Si is still indirect while the band structure for Ge is direct as can be seen in *figure 2.6*. Also, the corresponding density of states is plotted. In hexagonal Ge a direct bandgap is observed at the Γ-point.

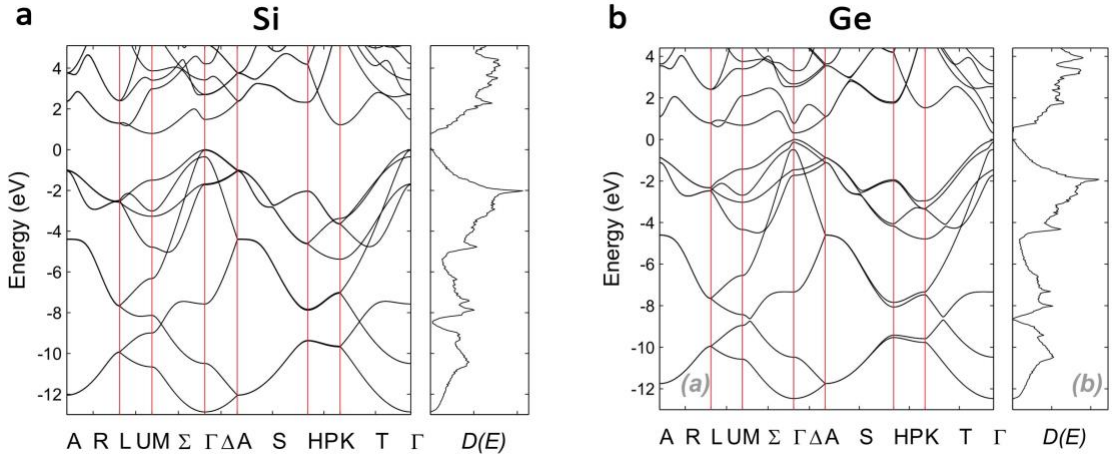

Figure 2.6 – The calculated band structure for and the corresponding density of states for hexagonal Si (a) and hexagonal Ge (b). Ge exhibits a direct bandgap at the Γ-point, while Si remains indirect. Image taken – De et al.[5]

Although the bandgap for hexagonal Ge is direct, not all the transitions from the conduction band to the valence band are dipole (quantum mechanically) allowed transitions. By going from the first conduction band with a Γ_8^- symmetry to the first valence band with Γ_9^- symmetry or to the second valence band with Γ_7^+ symmetry, these transitions are not allowed.[5] The only allowed transitions are from the second conduction band with Γ_7^+ symmetry to the first and second valence band as can be seen in *figure 2.7*.

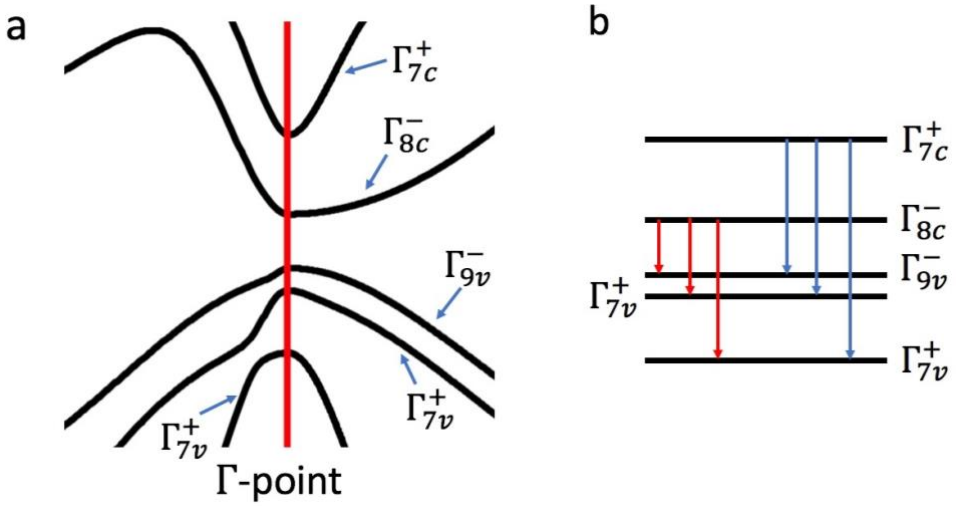

Figure 2.7 – A zoom-in of the hexagonal Ge direct band gap around the Γ- point (a). The only allowed transitions are from the second conduction band to at least the first three valence bands (b). The first conduction band has no dipole allowed transitions.

By alloying hexagonal silicon with hexagonal germanium an optically active semiconductor can be produced. For low Ge content in Si the Γ minimum in the conduction band is higher than the M minimum resulting in an indirect bandgap. This alloying of $Si_{1-x}Ge_x$, lowers Γ minimum compared to the M minimum. For a germanium concentration of 0% and 100% the position of the bandgap is calculated. By interpolating these number, the graph shown in *figure 2.*8 is derived. For x = 0.65 the Γ minimum and M minimum are assumed to be at the same energy level. This will result in having a direct bandgap when the Ge content is higher than 65%.

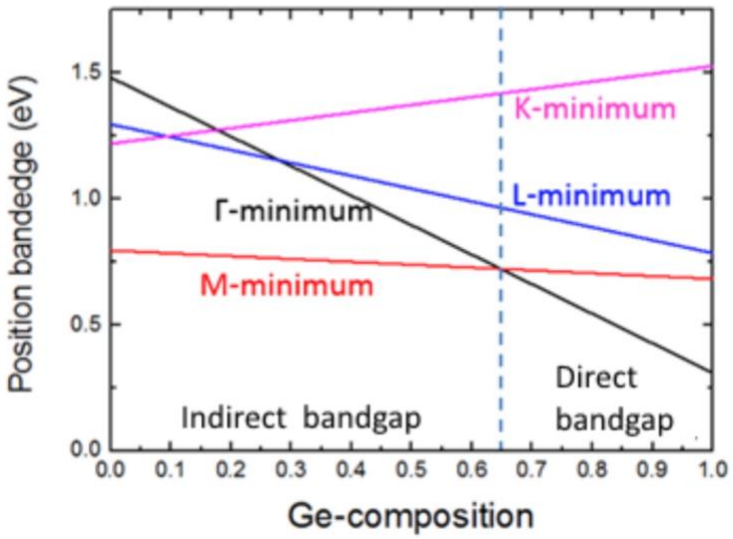

Figure 2.8 – Position of the bandgap for different Ge composition. The band gap becomes direct when the Γ minimum is below the M minimum. This is estimated to happen at a Ge content higher than 65% Image taken - Haverkort.

2.3 Growth mechanisms

All the nanowires grown in this work are grown via the vapor-liquid-solid (VLS) or vapor-solid mechanism (VS). In this section a brief introduction will be given explained on how the VLS growth mechanism works. Then epitaxial growth is explained and why it is necessary for branches and shell growth. Also, the mechanism for shell growth is explained. Further, the growth mechanism for different precursors is described and how this could relate to the growth kinetics of branches. And lastly, the currently investigated growth mechanism for branches is explained.

2.3.1 Vapor-liquid-solid growth

In this work nanowire are grown via the vapor-liquid-solid (VLS) growth mechanism by using a gold catalyst nanoparticle. Other nanoparticles can be used such as silver and copper[26] since Au can introduce deep-level traps in Si which is unfavorable for photoluminescence spectroscopy.[27] These deep-level traps can shorten non-radiative life time of charge carriers and can facilitate recombination of minority carriers. If the non-radiative lifetime is shorter than the radiative life time, then a carrier is more likely to combine non-radiatively.[28] This induces a phonon to be released instead of a photon and thus there is no light emission. The other method is used in this work to grow a Si shell is VS, which stands for vapor-solid mechanism. This method does not need a catalyst particle to crack the precursors efficiently but a high enough temperature to crack the precursor bonds.

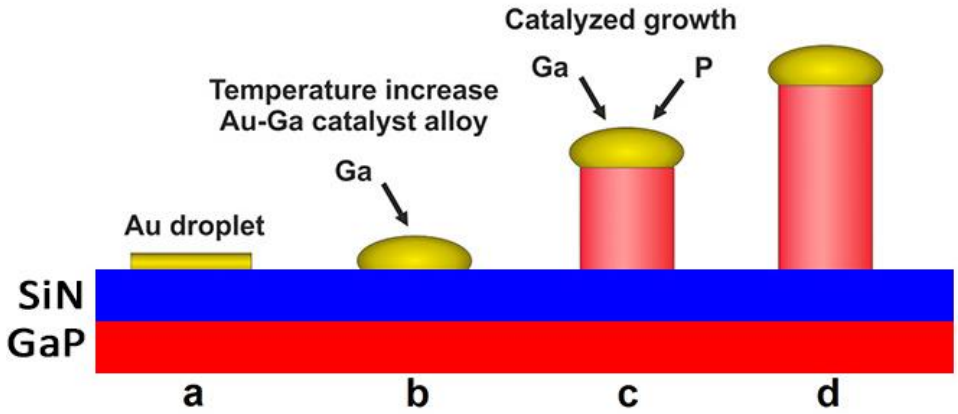

Figure 2.9 – The different stages during VLS growth. A layer of gold is deposited into the holes of the SiN mask patterned substrate (a). By heating the substrate and supplying TMGa precursor gas a eutectic alloy is formed between the Au-Ga (b). The supply of gas supersaturates the Au droplet and starts nucleation at the droplet/substrate interface (c) pushing the Au particle up by layer by layer growth growing a nanowire (d).

When a patterned substrate with gold disks is heated in the reactor, small AU droplets are formed. The size of the gold droplet determines the diameter of the nanowire. Since within the scope of this project nanoimprint lithography (for more info see *section 3.2.2*) is used to pattern the substrate, only one-hole size of around 130nm was used. To grow GaP core nanowires, TMGa is introduced in the reactor which forms a liquid Au-Ga alloy with the substrate. Group III elements are expected to form an alloy with gold, while group V elements are expected to be supplied from the vapor phase. When more precursor material is supplied, and the temperature is above the eutectic point, the nanodroplet will saturate and eventually supersaturate. This starts the nucleation at the droplet-substrate interface and more specifically at the vapor-liquid-solid line, which has been suggested to be one of the reasons that nanowire can grow WZ.[29] For more

information on WZ formation see *section 2.4.* This makes that layer by layer growth occurs under the gold droplet lifting the gold droplet up growing a nanowire. This process is graphically shown in *figure 2.10*.

In this way the metal gold particle acts as catalyst lowering the activation energy and the growth temperature. This can be seen in the fact that the decomposition temperature for disilane (Si_2H_6) is 640°C to grow a thin film. While the eutectic temperature for a Si-AU alloy is 363°C. This in contrast to melting points of Au and Si being 1064 °C and 1414 °C.[30]. The other precursor used in this work is Germane. Germane has decomposition temperature well below 300 °C depending on the pressure.[31]

2.3.2 Epitaxial shell growth

When growing the Si shell around the GaP core and the branches used in this project, epitaxy plays a very important role in growing the hexagonal crystal structure needed for the SiGe direct bandgap material. The word 'epitaxy' is derived from the Greek words 'epi' (on top of) and 'taxis' (ordered) and this method was first mentioned by Royer in the 1920s.[32] Epitaxy is a method to grow high quality crystalline surface which are determined by their crystalline orientation. During epitaxial growth, epitaxial films can be grown from the gaseous precursors in the MOVPE. Atoms from the gas phase diffuse across the surface. And since it is energetically more favorable to adhere to a step on the substrate and even more to adhere to a kink, new monolayers of high crystalline quality are grown.[33]

The substrate or in our case the side wall of the nanowire acts as a template, from which a layer is grown copying the crystal structure[12]. If an epitaxial film or layer is deposited of the same material, then it is called homoepitaxy. Otherwise it is called heteroepitaxy like the $Si_{x-1}Ge_x$ branches grown in this work. Below in *figure 2.11a,b* an example of good epitaxy of a Si shell on GaP is shown, similar to the nanowires used in this work. In which the crystal structure is copied from the GaP core to the Si shell. When growing the branches in the [1-100] or in the [11-20] direction as shown in *figure 2.1c,d*. The structural arrangement of ABABA stacking of the shell or the GaP will be preserved. This would be lost when trying to copy the crystal structure in the [0001]] direction since these direction does not contain information on the ABAB stacking order. Therefore, branches grown horizontally in this project are grown in an ideal direction to preserve the hexagonal crystal quality.

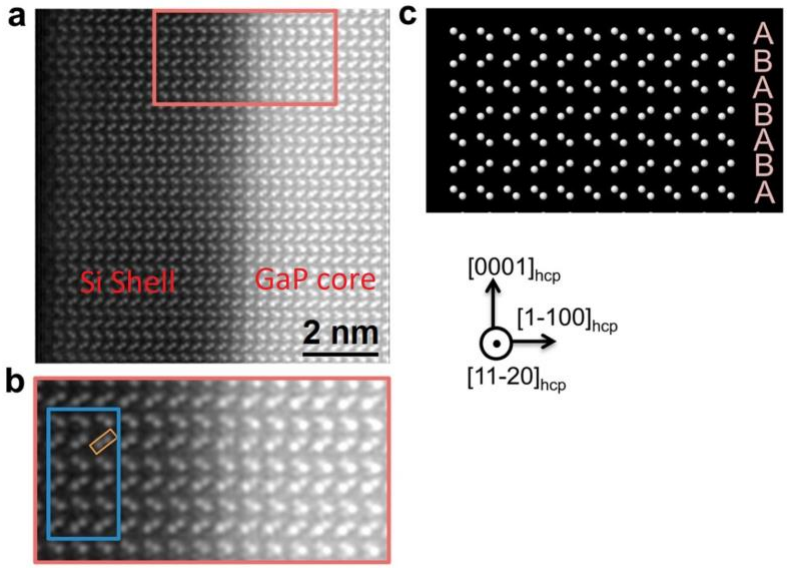

Figure 2.10 – A TEM image taken at the GaP/Si interface. (a) STEM image of the GaP/Si interface taken in the [11-20] direction. Left shows the Si shell and the lighter colored right side is the GaP core with Si shell. (b) A zoom-in of the orange box in (a). The orange box shows the characteristic dumbbell of WZ crystal structure when imaging in the [11-20] direction. (c) is a schematic representation of the structural model in (a). Images edited – Hauge et al [12]

Since axial and radial growth can be competitive process, they can happen simultaneously when being in the right growth regime. Shell growth occurs by the vapor-solid growth mechanism in which a thin film layer is deposited around a nanowire like a shell around a NW core. Generally, the VLS growth mechanism is initiated at a lower temperature than the shell growth regime. This is due to the catalytic effect of the gold particle, lowering the needed growth (nucleation) temperature. So, at higher growth temperature radial growth starts to play a larger role. Since during VLS growth the base of the NW is exposed longer to growth species than the freshly fabricated top. And there is diffusion of growth species coming from the substrate which is closer to the bottom than the top. The nanowires can be come tapered when growing a Si shell.[34] In our case the Si shell is thinner at the bottom than at the top.

2.3.3 Branches growth

When growing branches on the bare GaP cores or Gap cores with Si shell, the growth directions are different from the stems. The growth mechanics are the same since we use the same VLS growth mechanism to grow the branches. As earlier demonstrated the branches grow out in six equivalents <1-100> Azimuthal directions, see *figure 2.14a,b*.[17] The reason why branches are interesting is because they can grow in the hexagonal crystal structure when growing epitaxially on {11-20} side facets. One of the previous members of the group, Ang Li, has grown Ge branches on a Gap stem, shown in *figure 2.3.3c*. He showed that he could grow defect free branches which grow on the {11-20} side facets in the <1-100> direction. By taking a cross-section HRTEM image, the crystal structure and morphology is studied. The cross-section showed that the branch is tapered due to simultaneous vapor-solid shell growth, which results into the bottom and top {0001} facets having a cubic shell. Another reason why one could assume shell growth is occurring on the top and bottom facets of the branches is due to the fact that there is no cubic shell growth near the Au catalyst particle. This implies that shell growth originates from the nucleation of new layers on the {0001} side facets

rather than extending layers from the hexagonal trunk. The cross-section shows a rectangular shape, as is illustrated in *figure 2.14b.*

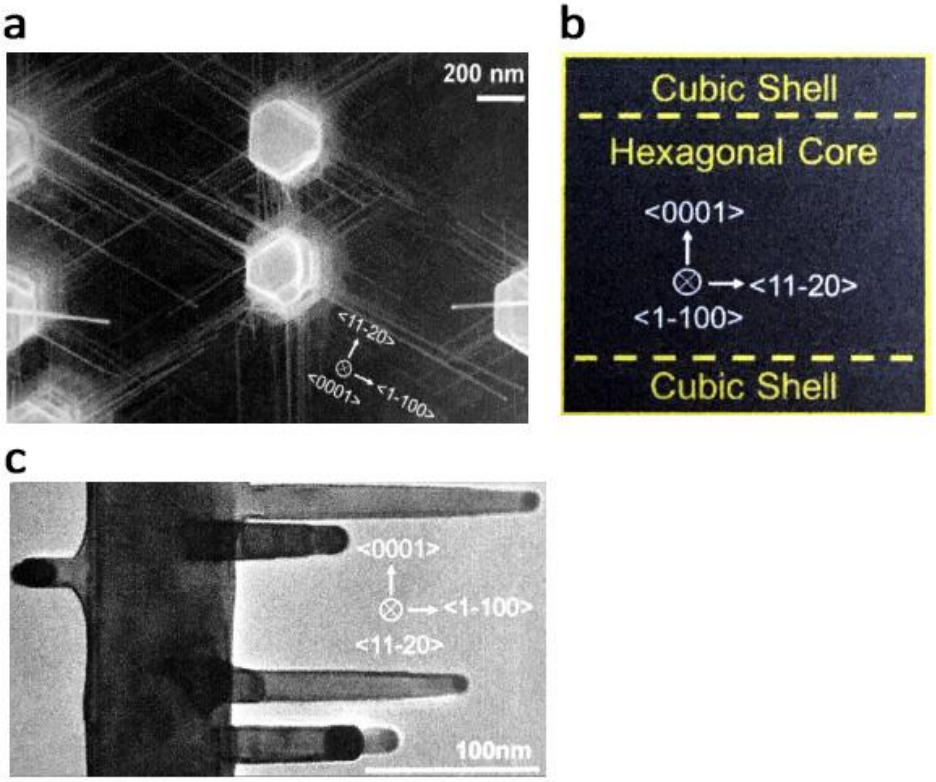

Figure 2.11 – (a) and (c) shows the <1-100> growth directions of the Ge branched nanowires on Si shell and the <11-20> side facets. (a) Shows a top-view SEM image and (b) a side view TEM image. To images these branches the <11-20> zone axis was used. (b) shows a schematic cross section of the branch showing the hexagonal VLS-grown nanowire along its axial axis with cubic top and bottom facets in the <0001> direction. Image taken – Hauge[17]

2.4 Parameters influencing the growth of WZ nanowires

The macroscopic properties of a nanowires e.g. light emission depend heavily on its crystal structure and thus the crystal structure of the branches used during this project. The formation of bulk crystal structures in III-V materials happens mostly in one specific crystal phase, while nanowires have variously been reported to be grown in different crystal phases.[35] The crystal phase can be influenced by the variations in diameter[36], unless wires they are very wide[37] or by adding dopants.[38] By changing the diameter or the doping this also heavily affects the nanowire properties, which causes unwanted side effects to the lasing and PL capabilities. In this section, two possible reasons are presented for the formation of a WZ crystal structure in nanowires. First a study by Joyce et al[13], who showed that under specific conditions only two basic growth parameters are influencing the promotion of the WZ crystal phase: Temperature and the V/III ratio. And a work by Glas et al[29], who showed that at the triple phase line due pertinent interface energies, Wurtzite nucleation is favored at high liquid supersaturation.

Joyce et Al showed experimentally that the most important parameters affecting the formation of WZ twinning layers is the temperature and the V/III ratio. A twinned bilayer could arise when the stacking sequence would change for example from ABCABCABC to ABCABACBA, in which a small wurtzite ABA segment is created,

and the order of layers is reversed. When every layer inside a ZB nanowire would be a twinned bilayer the crystal structure of the nanowire would be pure wurtzite. To promote the formation of these bilayers the twinning probability has to be increased so that at some point the majority of the crystal structure is WZ. As figure x shows, when increasing the temperature, the percentage of the twinned bilayers increased. When the V/III ratio was decreased this promoted the chance of forming a twinned Bilayers. So, a high temperature with a low V/III ratio gives the highest chance for forming WZ material.

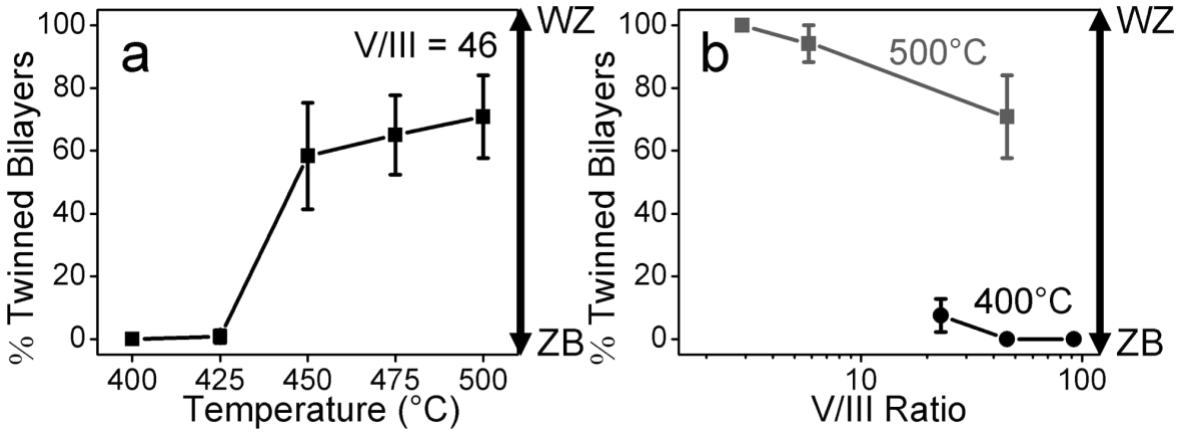

Figure 2.12 – The formation of WZ vs ZB by looking at the percentage of twinned bilayers by varying the temperature (a) and V/III Ratio (b). To promote WZ a high temperature with a low V/III ratio should be used. Image taken – Joyce et al[13]

Another way of explaining the origin of the WZ crystal structure in NW's is by looking at the nucleation point at the triple phase line. When a critical size of the gold droplet is reached the newly formed layer propagates over the entire surface forming one mono layer. The contact angle θ of the vapor-nucleus with respect to the vertical and β, the angle between the nanoparticle and the vapor phase influences the interfacial energy when a nucleus is formed. The angle of the nucleus can either be vertical, inward-inclined or outward-inclined as shown in *figure 2.16*. This interfacial energy gives rise to a change in enthalpy. The probability that a nucleus forms a twinned bilayer depends on the change in enthalpy and thus on the contact angles of the nucleus. While forming a nucleus at the triple phase line, WZ and ZB nuclei show major differences, which causes WZ formation to be favored for certain ranges of the relevant interface energies.[29] So, when the probability of forming a twin layer is high due to a high temperature or due to a high interfacial energy difference due to the right contact angle. Chances of forming a wurtzite crystal structure will become higher. When tuned to the right dimension and settings pure WZ nanowires can be formed.[13]

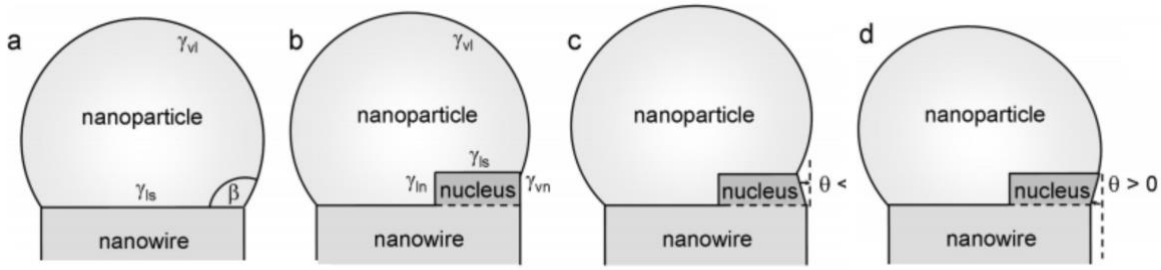

Figure 2.13 – Nucleation of a new layer in nanowire growth with a gold catalyst nanoparticle. A new nucleus can be formed the triple face line. In (a) β is the contact angle of the nanoparticle. The angle

of the nucleus with the gas phase can be flat (b), inward inclined ($\theta < 0$) *(c), outward inclined* ($\theta > 0$) *(d). Image edited – Joyce et al*[13]

2.4.1 Chemical deposition and precursors

The precursor kinetics play an important role in this project. Not only will we be growing Si branches from disilane (Si_2H_6) (Fig.2.12a), and tetrasilane (Si_2H_{10}) (Fig. 2.12b), but also trying to incorporate Ge into a Si branch by using the Si approach. Which means that we start optimizing a Si branch as the starting part point and then later start incorporating Ge into this optimized branch. Since there is only one Germanium (Germane, GeH_4) available in this work the main focus will be on the kinetics of the different Si precursors.

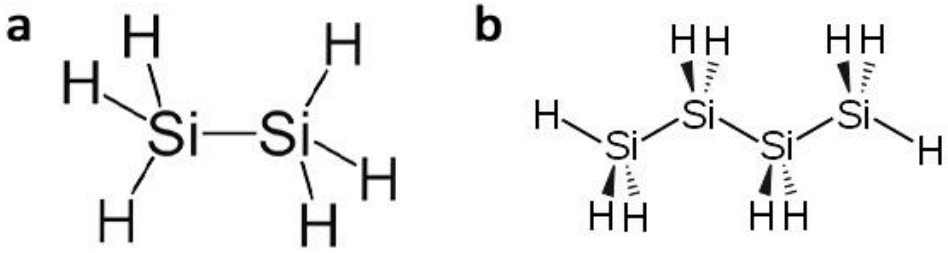

Figure 2.14 – Two different types of silanes used in this project. Dislane (a) and tetrasilan (b).

When comparing tetrasilane to disilane there is expected to be a distinct difference in the growth rate. Because the energy required to break the Si-H bond is about 3.9 eV compared to the single Si-Si bond which is about 2 eV. There is thus a tendency that the growth temperature can be reduced by changing to higher silanes. This can also be seen in the activation energy of the precursors. The activation energy of SiH_4, Si_2H_6, Si_3H_8, and Si_4H_{10} are 1.62 eV, 2.38 eV, 1.78 eV and 1.63 respectively.[39] For higher silanes the activation energy is steadily reduced. This is caused by the longer Si-Si chains which are more easily cracked in the reactor. The only exception is the silane precursor which is an indication that the detailed deposition mechanism is different compared to the higher silanes.[40] This also implies that the growth rate of higher order silanes is generally much higher as can be seen in *figure 2.13*. In which the growth rate is plotted for different orders of silane for our nanowire growth.

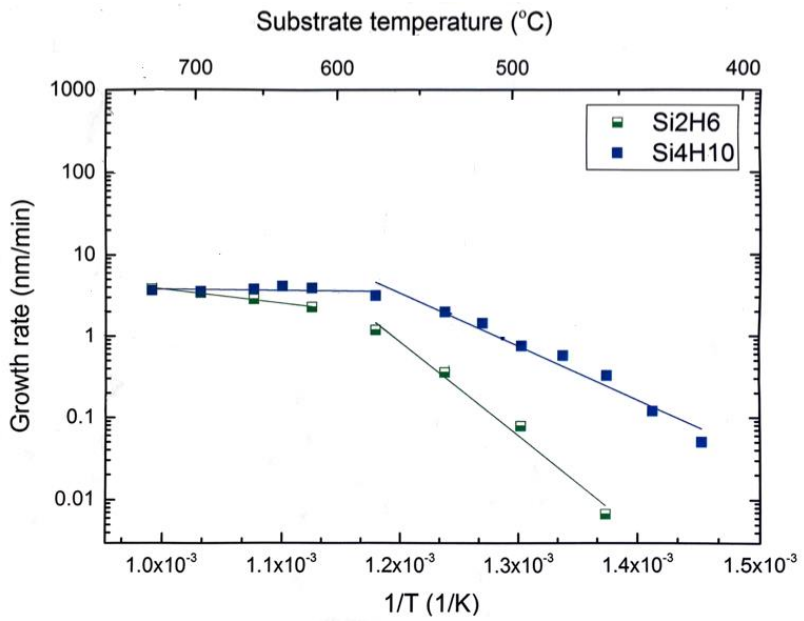

Figure 2.15 – Growth rate of a Si shell around a GaP core using silane and tetrasilane. The growth rate increases when the order of silane increases. Two regimes are visible below and above 650 ℃. Image taken – Ren.

To grow a Si nanowires with a disilane precursor it was discovered that the hydrogen desorption process is the major rate-limiting process both on Si(100) and Si(111) surfaces below 600 °C.[41] It was shown that substrate surface is covered with more hydrogens as the substrate temperature is lowered. This was done by measuring the QED spectra when thermally quenching the sample from its stationary state after 5 min. of epitaxy. And thus, the reaction is reaction rate limited. For higher temperatures the reaction is also reaction rate limited.[42] In this work the growth rate for disilane and tetrasilane will be compared, to check how different precursors affect the growth mechanism of branches. In this work the number of molecules are kept the same and thus the partial pressure of the precursor is the same.

2.5 Kinking of nanowire branches

In this work a lot of research has been done to kinking mechanism in SiGe branches. New insights in the kinking process asked more questions and raised possibilities for different experiments to be executed. Therefore, in this section will be described the different insights gained by reading different papers on the kinking process on similar systems and how this could affect the kinking mechanism in branches.

2.5.1 Angle of contact with catalyst particle and kinking of branches

Most nanowire heterostructures suffer interfacial gradients and kink formation during metal-assisted growth.[9,43] To achieve full control over the morphology and the properties of nanowires and nanowire branches it is important to understand the interaction at the interface between the metal catalyst particle and the formed nanowire. During the branches study done in this work many branches show a kinked behavior. One way to explain this phenomenon is when looking at a different nanowire system which show a similar kinking behavior, in this case InP and InAs heterostructure

nanowires. But has also been reported for many other materials systems.[44–47] Many research has been done to InP and InAs nanowires[48] and this might give a hint to the kinking process our Ge and Si branches in our nanowire system.

These studies show that in InP and InAs nanowires the sole parameter affecting the growth mode, in this case straight or kinked, is the nanoparticle composition.[48] This is regardless of what combination of precursor fluxes have led to the nanoparticle composition which was later determined by EDX. This flux commutation changes the composition of the NP and composition changes the stability of the nanoparticle. Kinking normally occurs when the Au nanoparticle tries to preserve the more stable interface during growth at the interface of the growing material. This is due to the different interfacial energies between the gold nanoparticle and the two-material system.[45] An increase of the in the In/Au ration leads to a corresponding increase of the size of the gold-Indium alloy and thus the contact angle increases. This relationship is shown in *equation 2* below, where V is the volume and β the contact angle of the NP. The volume of the gold droplet is determined by TEM images.

$$(\beta, R) = \frac{\pi R^3}{2\sin^3\beta}(2 - 3\cos\beta + \cos^3\beta) \qquad (2)$$

Thisperson et al reported that when the contact angle exceeds a critical value (in InP this 115 degrees) the VLS growth becomes unstable and the segment kinks. Straight nanowires can only be formed if the In/Au ratio in the nanoparticles is low, which is typically smaller than 1.5. For higher ratios the nanowires show kinked behavior. The ratio of In/Au during these experiments was tailored by the flux of available precursors at a fixed growth temperature which resulted in straight and radius-uniform InAs-InP nanowire heterostructures with atomically sharp interfaces. Below in *figure 2.17* is the relationship between the contact angle and surface energy difference plotted. As well as the different regimes for growing narrowing, vertical, widening and kinked nanowires.

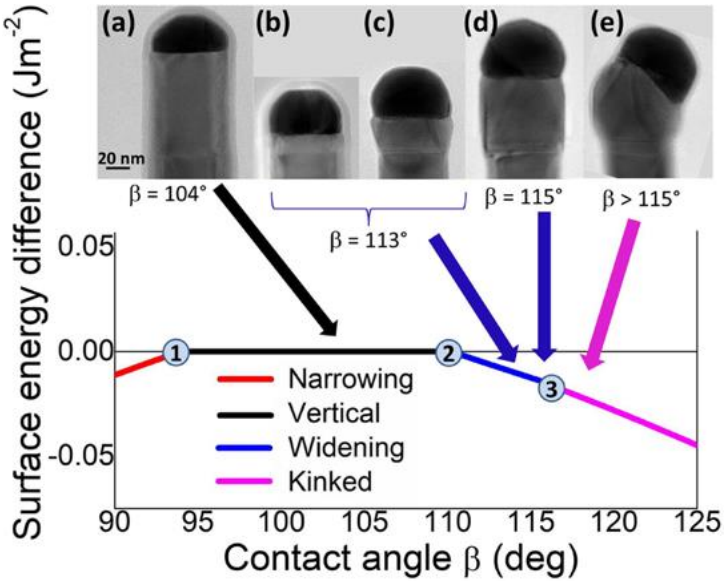

Figure 2.16 – The surface energy difference plotted against the contact angle of the Au/nanowire interface in InP nanowires. Below point 1 the nanowire is Narrowing, between point 1 and 2 the growth is vertical, widening between point 2 and 2 and kinking after point three, which corresponds with a

contact angle of larger than 115°. In the inserts representative TEM image are shown. Image taken – Zannier et al[48]

By changing the nanowire/nanoparticle interfacial configurations. The nanoparticle stability can be changed and thus the crystal phase trends and abruptness at the interface can occur. Therefore, we could assume that the kinking in the branches can be caused by a too highly saturated gold particle. This principle is proven in *chapter 4.5.* by changing the flow which saturates the gold particle.

2.5.2 Angle and kinking frequency

Another way to looking at the kinking process within the nanowire branch is by checking the crystal direction of the joint and the kinking angle. As shown by Bozhi Tian et al, in order to grow kinked or zigzag nanowires, the straight segments are joined together by triangular joints. We're interested in this system because their system has a lot of similarities to our kinked branches. They use the same material, both are in the cubic <111> plane, both systems use an Au catalyst particle. It's about the same dimensions and they have tried their theory with III-V hexagonal semiconductor materials. They showed by changing the gold droplet concentration of Si in-plane nanowires that they could kink the nanowire by depleting the gold droplet and making the nanowire unstable. In this way they could control the number of kinks and the spacing between the kinks.

This was done in three main steps during nanocluster-catalyzed growth shown in *figure 2.18a*. Axial growth to grow an arm segment (1), purging of gaseous reactants to suspend nanowire growth and depletion of the gold droplet while perturbating the growing direction (2), and supersaturation and nucleation of nanowire growth with the re-introduction of the reactants (3). By doing steps (1)-(3) a second building unit (SBU) can be formed, which connects to tow arms by a fixed angle joint. The formation of a kinked can be explained by the stepwise model shown in *figure 2.18*. In which first the concentration of the reactant in the gold particle drops, stopping the nucleation process. Then the reactant is re-introduced and the Au NP becomes supersaturated again, which proceeds growth with preservation of the most stable $\{111\}_c$ /$\{0001\}_h$ facets, which implies that nucleation happens at the active $\{110\}_c$ /$\{1\text{-}100\}_h$ facet of the three face boundary.[49,50]

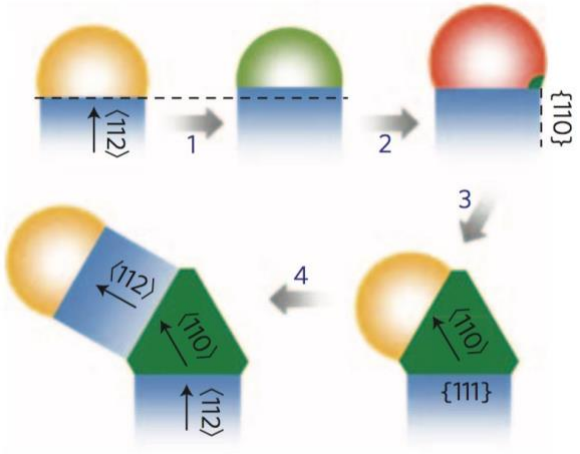

Figure 2.17 – The process during the kinking formation. First the gold droplet is depleted (1) until the reaction stops (2). The gasses are re-introduced, and nucleation happens at the least stable <110>

interface (3). Which concludes at growing a triangular joint structure at which nucleation happens again to continue growth <112> crystal direction (4). Image taken – Lieber et al.[50]

When comparing the growth before, during and after kinking it shows that a single crystalline is present across the entire SBU. This is in contrast to other modulated nanowires such as twinning superlattices.[51,52] The joint which connects the two arms has a quasi-triangular structure with {111} or {0001} bottom/top facets and two $<112>_c$ or $<11\text{-}20>_h$ facets connecting the two arms. Note that the vectors $<112>_c$ or $<110>_c$ in a cubic lattice are the same as the $<11\text{-}20>_h$ or $<1\text{-}100>_h$ in a hexagonal lattice when rotating about the $<111>_c$ or $<0001>_h$ zone axes. In a cubic system growth along the <110> is short lived since it is not thermodynamically favorable in this diameter regime. Which is mostly reserved for the very small sub 20nm diameters.[53] Thus the transition is happening from $<112>_{arm}$ to $<110>_{joint}$ to $<112>_{arm}$ giving a kinking angle of 120° as shown in *figure 2.19*.

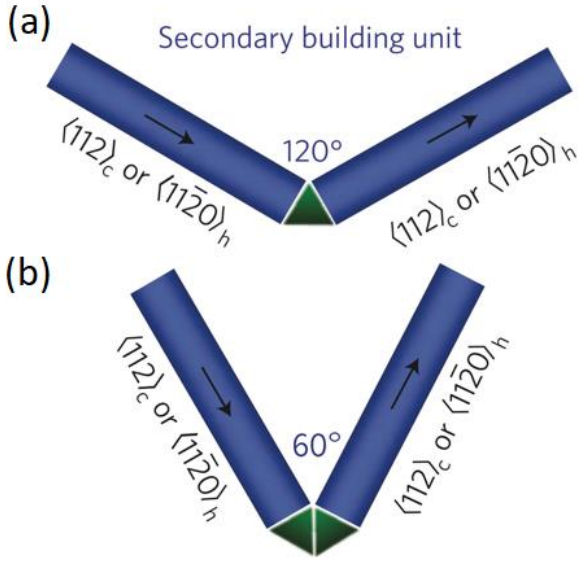

Figure 2.18 – Two schematic overviews of an expected secondary building unit. The top SBU (a) having an angle of 120° and one triangular joint and the bottom SBU (b) having an angle of 60° and having two triangular joints. Both systems having their arms within the same crystal directions and are single crystalline across the arm-joint-arm structure. (a) Is described in literature, while (b) is the expected structure for creating a 60° angle. Image edited – Lieber et al[50]

By implying that the triangular joint is formed between the two arms, we could speculate that a joint of 60° is possible by connecting two triangular joints. The SBU is also predicted to be true in other materials such as the wurtzite phase of the group II-V semiconductor CdS and group III-V nanowire materials such as GaN where all the arms are reported to lie purely in the <11-20> crystal orientation.[54]

When depleting the gold droplet not all the wires kinked, but only a specific percentage of the number of purges defined by the kink frequency. This frequency is defined as $P_{kink} = N_k/N_t = N_k/(N_k+N_s)$, where Nt, Nk and Ns denote the number of total designed junctions, observed kinks and observed straight and node-like junctions respectively. This kinking frequency was measured for two different wire thicknesses, 80 and 150nm. In which the thicker wire showed a less kinking behavior as can be seen in figure 2.20b. Also, the purge time is important for the kinking frequency, with a lower purge duration giving a lower kinking probability. This kinking probability can also be seen under the SEM in figure 2.20c, where the yellow stars indicate the position where the purging of reactants happened, but the nanowire didn't kink. So, there is always a

probability of kinking occurring, which makes the implication that there is also a chance that the nanowire might kink randomly. Given that branches are relatively thin, around 50nm compared to the 80 to 150nm Si wires used in the paper of Lieber et al, we expect that the branches in this work have a high kinking probability. Also shown was that the segment length of the arm can be varied by changing the growth time. This segment length scales linearly with the growth time as can be seen in figure 2.20 e. and figure 2.20d. In which the growth time is decreased going from (6) to (1).

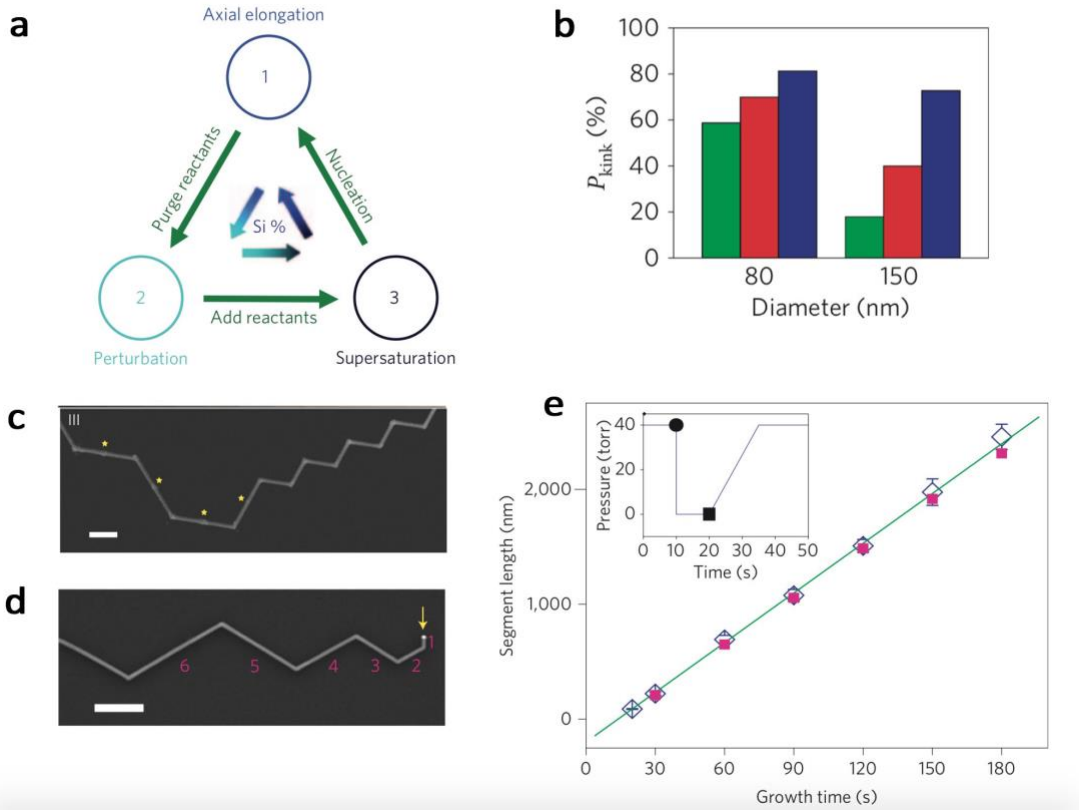

Figure 2.19 –(a) Represents the cycle for SBU synthesis. The inner blue arrows represent the Si concentration where dark blue is highest and light blue lowest. (b) The kinking frequency measure for two different thickness of nanowires at three different purge durations, 1 sec. (green.), 3 sec. (red.) and 15 sec. (blue) averaged over at least 15 multiple kinked nanowires. (c) SEM image of modulated kinked nanowires and incipient kinks marked with a star. The scalebar represents 1 μm. (d) SEM image of different growth times from 30 to 180 seconds in which the growth time is increased from segment 1 to 6. The scalebar represents 1 μm. (e) shows the growth time plotted against the segment length giving a linear relationship. The inset gives a representation of the purging cycle where the time is plotted against the growth pressure. Herby the black solid sphere and square denote the start of the purge and the reintroduction of the reactants respectively. Image edited – Lieber et al[50]

3 Experimental Methods

3.1 A summary of processing

To grow branches, first wurtzite GaP nanowires were grown, which act as a template for the epitaxial growth of the hexagonal structure in the branches. Nanowire fabrication consists of series of complex fabrication techniques to grow the GaP stems used. First a GaP (111) wafer is cleaned in phosphoric acid (H3PO4 : H2O = 1:10) for 5 minutes to get rid of the oxides present on the wafer. Then a selective area mask is deposited by using plasma-enhanced chemical vapor deposition, described in *section 3.2*.1. The mask used is silicon nitride (Si_3N_4) which is deposited on both side of the wafer to reduce the amount of GaP exposed. Then a layer of PMMA is applied with the spin coater and hardened. A nanoimprint stamp is used to define the pattern, which is described in *section 3.2.2*. Before using the stamp, a small sol-gel layer is applied. The stamp is then applied and left to set for 3 hours, in which the sol-gel is hardened tot glass silica. The layer of sol-gel and PMMA gets compressed by the pillars of nanoimprint stamp. And thus, the thickness of the sol-gel layer and the PMMA which get compressed is thinner than the uncompressed part of PMMA and silica.

Next the mask is etched by using reactive ion etching (RIE). The thicker layer of Sol-gel and PMMA acts as a protection for the underlying layer of silicon nitride. In this way, only the places where the nanowire pillars were present are etched and thus masking out the holes for nanowire growth. By evaporating 10nm of gold onto the substrate, see *section 3.2.3*, gold is deposited into the now defined holes on top of the GAP wafer and the resist layer. By lifting of this resist layer in organic solvent, the substrate is patterned with gold filled holes and a silicon nitride mask.

Before nanowire growth the mask is cleaned in sulfuric acid and Piranha to etch away the oxides and organic solvents. Then the nanowires are grown in a metal-organic vapor phase epitaxy (MOVPE) reactor. After growth the nanowires were taken out of the reactor and their Au catalysts droplets are etched by using Kings water and KI/I^- solution, see *section 3.2.4*. Then a Si shell could be grown in the MOVPE reactor depending on the experiment. Next the oxides were removed by performing a HF dip before depositing 10nm of AU onto the grown nanowires. Finally, the branches were grown by using the MOVPE reactor, described in *section 3.2.5*. The layer of gold deposited on the sidewalls is used as a catalyst particle for the SiGe branches of the nanowire. Which are then grown inside the MOVPE reactor.

3.2 Substrate patterning

3.2.1 Mask and resist application

To pattern the substrate first a silicon nitride (Si_3N_4) masking layer is applied on a GaP (111) wafer to prevent parasitic nanowire growth and to promote faster surface diffusion. This dielectric layer is crucial in this work since it prevents wires emerging from the substrate when we deposit gold for the second time before growing the branches. This was done by using plasma-enhanced chemical vapor deposition (PECVD). This technique uses a plasma, which is (partially) ionized gas which consists of electrons and ions. In this reactor a sold cold plasma is used, which implies that the temperature of electrons is higher than the temperature of ions and neutral molecules. This is due to electrical ionization by radio frequency electric field and thus no heating of the substrate is needed. Since the energy of the electrons is high, they can decompose the precursors into radicals. These radicals will diffuse to the substrate surface and form a thin film. The PECVD used is from Oxford Instruments and deposits 100nm Si_3N_4 mask. The thickness of the mask is verified by a refractometer which measures the index of refraction by using Snell's law. The standard waveguide program used has an input flow of 17sscm Si_3N_4, 13sccm of NH_3 and 980 sccm of N_2, which gives a total flow of 1010 sccm. The radio frequency source operates at 13.56MHz, while the pressure inside is 650mTorr.

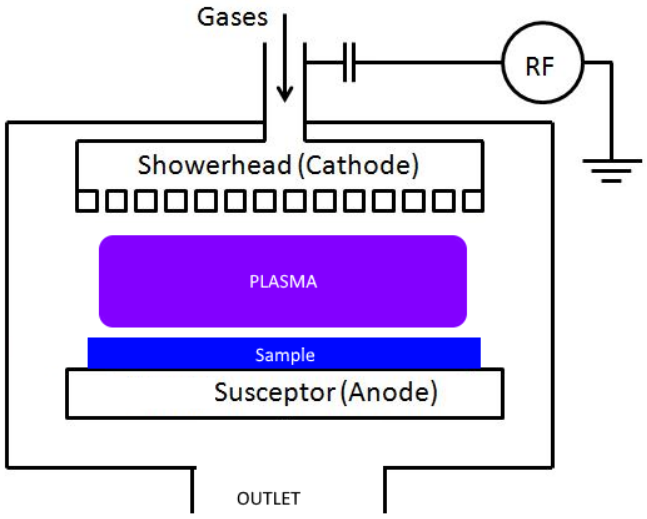

Figure 3.1 – The schematic overview of a PECVD. The radio frequency (RF) source works at 13.56Mhz producing a plasma. A showerhead injects the precursors gasses at the top and the sample is placed on top of the susceptor. The radical ions are moving from top to bottom form a thin at the bottom. The excess precursor particles leave the chamber via the outlet at the bottom.

Then a second layer of PMMA is deposited on top of the silicon nitride mask. Polymethylmethacrylate (PMMA) is an insulating polymer which can be used as photoresist. Also, it is highly soluble in acetone which makes it possible to dissolve the layer easily when doing lift-off. The PMMA used during this work is RNR-I PMMA 35K-300. The PMMA layer is applied by spin coating at 3000 rpm, with an acceleration of 10.000 rpm for 57 seconds. After this the substrate is bakes at 150°C for 15 min. This results into a PMMA layer of around 300nm.

3.2.2 Nano imprint

There are two common ways to pattern wafers with a regular array of catalyst particles intended for VLS growth. Electron beam lithography (EBL) and nanoimprint lithography. During the scope of this project use has been made of nanoimprint lithography, since the recipes developed within in the group are stable and serve the purpose of growing almost defect free GaP cores with or without Si shells needed to grow high quality branches. Also, it is fast compared to EBL and for that reason it can be applied more easily in industrial applications. The disadvantages of nanoimprint lithography are that this method is not flexible in terms of its pitch size, hole size and geometric position of wires since it relies on use of a master patterning mask. This master is expensive and can only be used for a whole wafer. Earlier experiments performed have shown that the results are reproducible for an entire wafer and there are no significant differences between the center and edge of the wafer.

The master stamp is created by making use of a Si wafer which functions as a negative master pattern. This master pattern which contains arrays of holes is fabricated by EBL and this pattern is then transferred onto a flexible polydimethylsoloxane (PDMS) Stamp. The final result is a flexible stamp containing a regular array of protruding pillars[55] with a pitch of 2.5 microns and a diameter of 250nm used in this project.

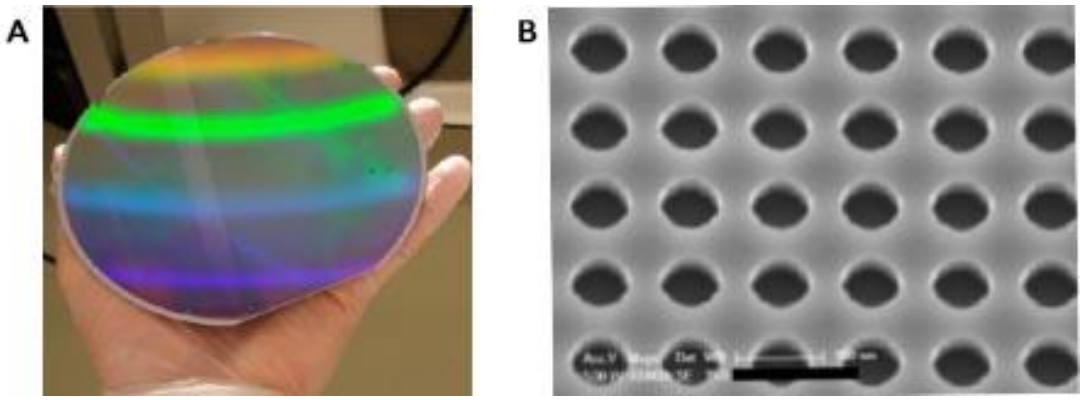

Figure 3.2 – (a) Example of PDMS nanoimprint with uniform interference color bands in the stamp used to pattern a 2" wafer. (b) Result after applying the nanoimprint stamp, where uniform arrays of holes are visible. The pattern used during this project has a different lay-out than show in the SEM picture. Image taken - Verschuuren[55]

To pattern the substrate a layer of sol-gel imprint resist of tetramethoxyorthosilicate (TMOS) and methyltrimethoxysilane (MTMS) is spin coated onto the PMMA. Within 1 min, when the sol-gel layer is still liquid the PDMS is applied and left for 3 hours. Due to the capillary force the features in the stamp are filled with the sol-gel resist. After 3 hours the PDMS stamp is peeled off leaving the full 2" wafer patterned with an array of wholes as shown in *figure 3.2b.*

Since there is a difference in thickness between the compressed sol-gel layer by the nanoimprint stamp and the sol-gel layer, the compressed layer will need less etching time to reach the PMMA layer. By applying this principle, it is possible to reach the gallium phosphide wafer before removing the PMMA resist layer which is necessary for the lift-off of the excess gold. This is achieved by using reactive ion etching (RIE) to transfer the design onto the GaP wafer. During the RIE, argon gas and 50sscm of CHF_3 are introduced into the reaction chamber which operates at 15 mTorr. By applying a RF signal at 13.56 Mhz the argon gas gets decomposed into Ar^+ and

electrons, while the CHF_3 decomposes into F atoms, CF_2 radicals and CHF_2^+ ions. The positive ions are then accelerated towards the anode where the substrate is positioned and thus bombarding the surface of the wafer. This bombardment results in anisotropic etching of the surface.

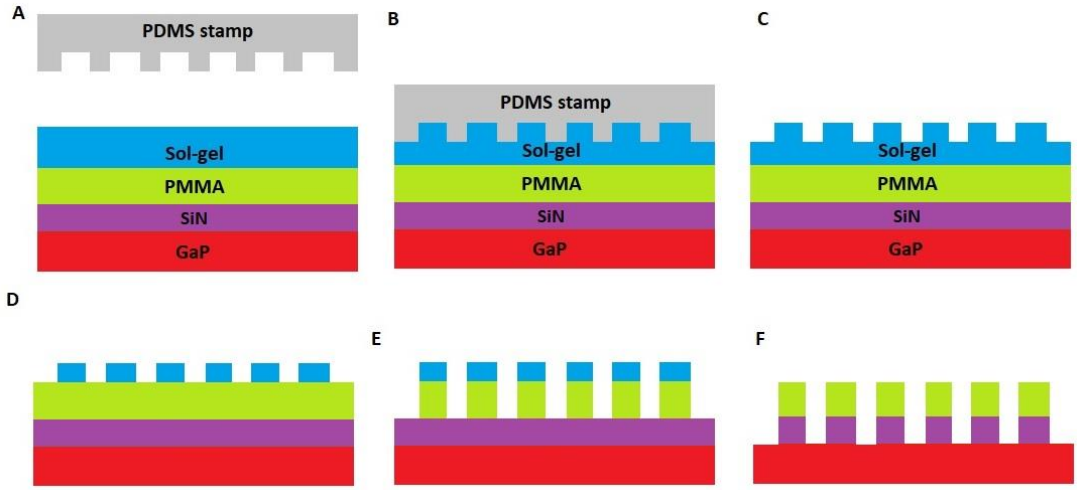

Figure 3.3 – The process of nano imprint lithography. (a) The PDMS stamp is applied onto the liquid sol-gel resist (b). The PDMS stamp is pealed of (c) and then etch with the nitride RIE until the PMMA layer is reached (d). Then the PMMA layer is etched with the polymer RIE until the SiN is exposed (e). Then the last layer of SiN is etched until the GaP is exposed (f).

By etching the right amount of time, the GaP wafer is exposed, while preserving the PMMA layer. This layer can be lifted of after AU deposition is done. This is achieved by dry etching the silica with reactive ion etching (RIE) for 40 seconds. Then using the polymer RIE to dry etch trough the PMMA layer for 3.5 minutes. Although there is no limit to the etching time of the PMMA layer, it shouldn't be overdone, because it etches the SiO_2 layer physically. Lastly, the nitride RIE is used to etch trough the final layer of SiNx to expose the GaP wafer. These steps expose the Gap wafer while preserving the SiN mask and PMMA layer.

3.2.3 Gold evaporation and wafer preparation

During the substrate processing gold is evaporated two times onto the substrate before growth. The First time is before growth of the GaP core nanowires. The excess gold is lifted of before growth by dissolving the PMMA Layer. After the GaP cores are grown, the gold droplet is etched which is described in *section 3.2.4*. Then a Si shell is grown of around 20 nm, which is inversely tapered to the tapering of GaP core. After the Si shell growth, a 10nm layer of gold is deposited at 45° angle as shown in *figure 3.5*. After the 2nd gold deposition the branches are grown via the VLS is mechanism. The gold is deposited by using the electron beam evaporator. Substrates are placed upside-down onto a substrate holder which is placed in the load lock. Samples are clamped onto the substrate holder with small metal pins. This will always give a mask on the substrate which prevents branches growth on the masked region due to the lack of gold.

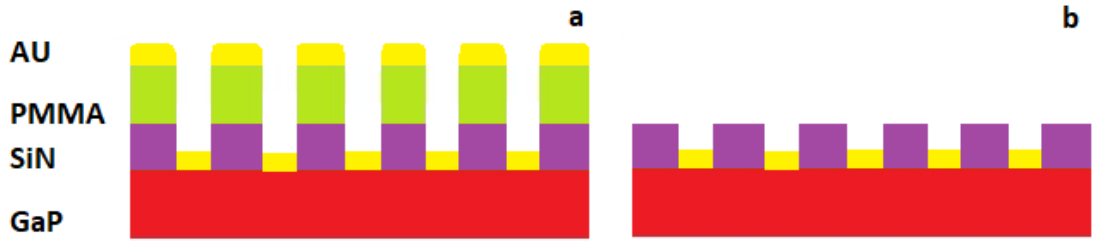

Figure 3.4 – After the gold is deposited (a) the layer of PMMA gets dissolved in acetone. This removes the unwanted gold and leaves a patterned substrate with gold discs deposited in the holes of the SiN mask (b).

Electrons emitted by an electron gun are focused by an electric field onto a cubicle containing the metal to be evaporated. When the metal gets hot enough it starts evaporating. A shutter controls the deposition time when the evaporation flux is tuned to the needed deposition rate. The evaporation beam is very directional, and for that reason Au on the GaP/Si shell nanowires are deposited onto a 45° angles, as shown in *figure 3.5*. Otherwise no gold would be deposited on the side walls, but solely the top segment of the nanowire. When heating up the sample the gold is melted and is distributed evenly on the sidewalls.

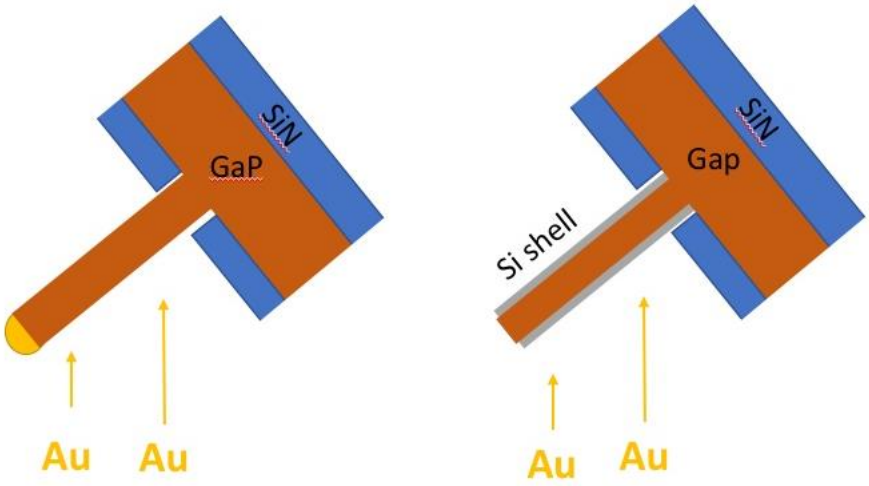

Figure 3.5 – Gold deposition on 45° angle for a substrate with and without a Si shell. Gold deposited on the side walls of the nanowires. When the substrate is heated, the gold film will distribute evenly over the entire surface of the nanowire forming blobs which can be used as an Au catalyst during VLS growth.

Before the wafer can be used for growth, all the organics are removed in piranha 4:1:1 (4 H_2SO_4 20mL, 1 H_2O 5mL, 1 H_2O_2 5 mL) solution. First the pieces are dipped in sulfuric acid for around 5 seconds. Then they are dipped in piranha solution for 45 seconds and then they are dipped again pure sulfuric acid for 5 seconds. Then the wafer pieces are rinsed in DI water until PH is neutral. This processing makes sure that all the organics are removed. Before growing the nanowires, the surface oxides are removed by doing a phosphoric acid dip for 45 seconds. And then rinsing with DI water until the resistance of the water is higher than 8 MΩ*cm. Before the gold is deposited for the branches the pieces are dipped in 10% HF to remove the oxides.

3.2.4 Gold etching

In order to grow a silicon shell around the GaP core, the gold has to be removed since it causes axial growth of Si on top of the GaP core. This is done by wet etching the gold droplet by using potassium-iodide/iodine (KI/I_2) solution. To etch the gold first the

substrate is placed in diluted phosphoric acid, H_3PO_4(85%):H_2O (1:1) for 30 seconds to wet the surface and to remove the oxide layer on the gold droplet. Then the sample is placed for 45 seconds in diluted king's water, HCl(36%):HNO_3(65%):H_2O (3:2:6). Since the gold droplet was used as a gold catalyst during nanowire growth the gold droplet is filled with gallium and has an outer gallium crust. The king's water helps in removing this crust to expose the gold, so it can be accessed more easily by the KI/I_2 solution. Then the substrate is placed in potassium iodine/iodine solution for 12 min. in which the gold is etched. Because the activity of the KI/I_2 solution increases over time it is important that the samples are placed into the solution after no more than 30 minutes after preparing it.

During the etching process the samples were rinsed in for 10 dips in a 1L H_2O beaker. After the etching procedure the gold residue was removed by rinsing in three different H_2O beakers. Then it was placed in beaker with a magnetic stir bar which spins at 250 rpm, while flushing with UPW water at room temperature for half an hour. After the rinsing the wires were dried by placing them in IPA. IPA has a lower surface tension than water and thus prevents the wires from breaking off while spin-drying them for 30 seconds at 7000 rpm.

3.2.5 Metal-organic Vapor-Phase Epitaxy

The nanowires are grown in a metal-organic vapor phase epitaxy (MOVPE) reactor. This is a chemical vapor deposition method in which crystals are grown by chemical reaction and not by physical deposition as used in molecular beam epitaxy (MBE). In the MOVPE two types of precursors are used: the metalorganics for group III elements and hydrides for group IV and group V elements, such as trimethylgallium (group III) and disilane (group IV). For metal organics mostly, a hydrogen carrier gas is used to carry the precursors from the bubblers into the reactor. Below in *figure 3.6* a schematic overview of a showerhead of an MOVPE reactor is shown. The precursors gas is injected from above the substrate via the ejection through many small holes which ensures an even distribution across the surface. This happens while the substrate slowly rotates around its axis for an even better gas distribution.

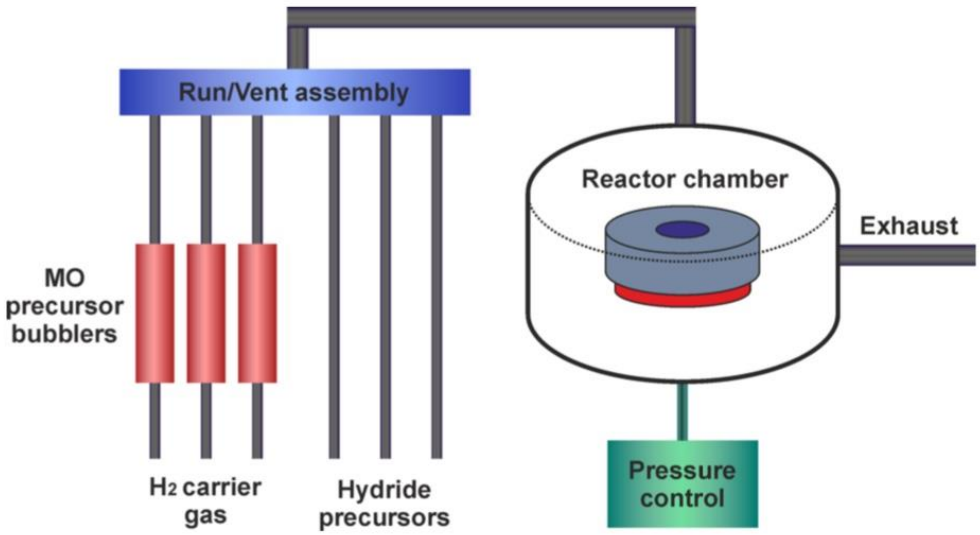

Figure 3.6 – A schematic of a MOVPE reactor. Two types of precursors are used, metal-organics (MO) and hydrides. In this setup a shower head is used which injects the gas from the top on to the susceptor and is pumped away via the exhaust. Image taken - Assali[56]

The susceptor is made of graphite and can hold a 2" wafer. Smaller samples are placed between Si dummy pieces to prevent deposition on the susceptor and to enhance the surface diffusion, so that the growth conditions between different runs are kept the same. The pressure is controlled by a pressure controller and is varied between 25 and 50mbar during the experiments. The total pressure in the reactor is determined by the partial pressure of the source materials and thus the pressure influences the deposition rate. A resistive heater with different heating zones ensures a uniform temperature profile across the entire surface of substrate. All the temperatures reported in this work are input temperatures. Since the heater and the thermocouple are placed millimeters apart, this will result into a temperature difference. Normally the real temperature of the substrate is around 100°C lower than the input temperature. Other variables used are the flow of the precursors, growth time, annealing steps and different growth schemes. In this work we do not bother on the V/III ratio of GaP as it is kept constant during the entire work.

In this work, the precursor Poshphine (PH_3) and trimethylgallium (TMGa) are cracked to individual molecules and are used via VLS growth to form epitaxially grown nanowires. A minimal 570°C temperature is needed to crack TMGa and PH_3.[57] Generally, hydrides have a higher decomposition temperature than metal-organics.[58] More about the cracking temperatures of other precursors used can be found in theory *section 2.3.1* and *section 2.4.1*. Other precursors such as Disilane (Si_2H_6), Tetrasilane (Si_4H_{10}) and Germane (GeH_4) are used to grow the shells and the branches of the nanowires. Hydrogen Chloride (HCl) gas was introduced into the reaction chamber to prevent tapering of the nanowire when growing germanium branches.[59]

3.3 Analysis techniques

During this work use has been made of two different characterization techniques: Scanning Electron Microscopy (SEM) and Transmission Electron Microscopy (TEM). The SEM is used to image the outer morphology of the GaP cores, the Si shell and the branches. As well as for analyzing the branches in terms of length, width, tapering and doing statistics on the kinking angle and frequency. The TEM is used to investigate the crystal structure of the nanowires and to check for defects in terms of cracks and stacking faults.

3.3.1 Scanning Electron Microscope

The scanning electron microscope (SEM) is used in this work to investigate and measure the branched nanowires morphology and dimensions. In the SEM electrons are accelerated from a field-emission electron gun and focus onto the substrate. Electrons have a much smaller wave length than an optical microscope and thus a SEM can give a much higher magnification (up to 300.000x), which is much higher than the optical limit. The electrons emitted travel through a series of electromagnetic lenses and are focused onto the sample. When the electrons hit the surface, the electrons can penetrate (~micron) into the surface and are deflected. This process causes secondary electrons and back-scattered electrons, which are collected by a detector as can be seen in *figure 3.7*.

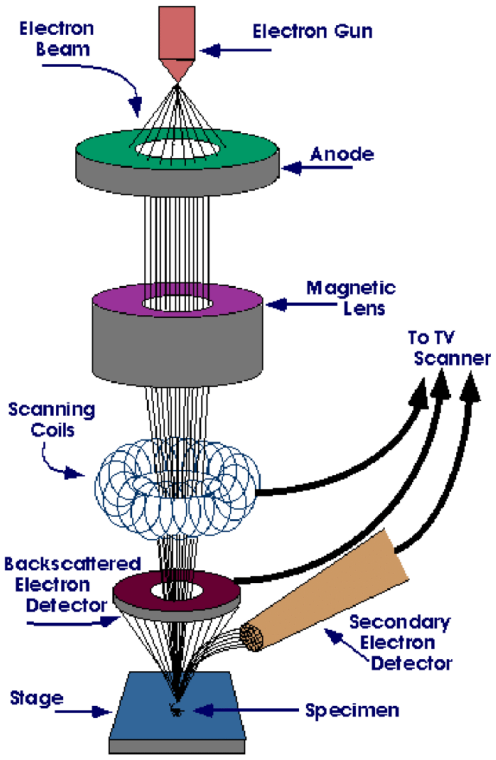

Figure 3.7 – Schematic overview of a scanning electron microscope. Electrons are emitted from an electron gun are focused through a magnetic lens onto the substrate. After the electrons hit the sample the backscattered electrons and secondary electrons are collected by their own detectors. Image taken – reserachgate.net[60]

The SEM operates at vacuum at a pressure lower than $5*10^{-5}$ Torr. The SEM used during this project is a Zeiss Sigma, and measured at a bias of 3 kV. The measurements are done with the Inlens detector at an angle of 0°, 30° and 90°. The angle at zero degrees is used to calculate the length of the branches, to make an estimation of the yield and the kinking angle and the number of kinks per micron. A thirty-degree angle is used to study the point of nucleation at the interface between the stem and the branch. The ninety-degree angle is used to study the density of branches across the stem, the tapering of the branches and the to check for substrate growth. In order to image the sides of the branches, the wafer has to be cleaved at a ninety-degree angle. When cleaving the sample, it is possible to check the side of the substrate for substrate deposition.

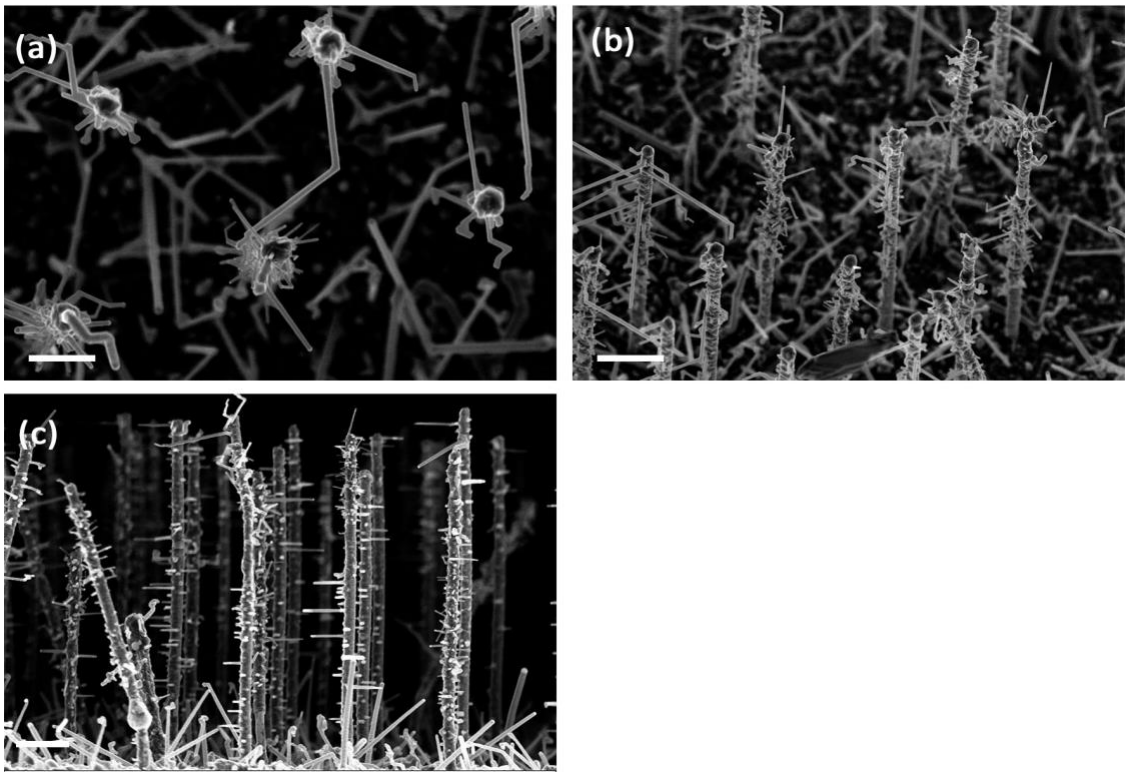

Figure 3.8 – The branched nanowires images at three different angles. From the top view (a), which makes it possible to image the tapering and length and width. At a 30 ° angle (b) to image the point of nucleation. And from the sideview (c) which allows to image the substrate growth. The scale bar represents 1 micron.

3.3.2 Transmission Electron Microscopy

Transmission electron microscopy (TEM) operates in a similar way as the SEM, but in a TEM electrons are accelerated with a much higher potential in the order of hundreds of kV. The TEM can reach a much higher resolution down to about 50pm, enough to be able to resolve atoms in a crystalline structure. In this way it is possible to image the atomic arrangements, the crystal structure. But also, the quality of the crystal lattice in terms of cracks and defects. In contrast to the SEM, in the TEM electrons are transmitted through the sample and not just scanned across the surface.

The TEM magnetic lenses are used to guide the electrons through the column and through the sample where the scattering of electrons occurs. The angle of convergence can easily be changed by changing the current through the coils. In bright field TEM mode the electrons passing through the sample are measured with an objective aperture placed in the back focal plane, which focuses electrons on CCD camera. A TEM has from bright field also other different modes in which it can operate. The different modes available have their own advantages in imaging the crystal lattice. In High-resolution TEM (HRTEM) the transmitted and scattered beam are used to form an image containing lattice fringes. Although these fringes are not a direct image of the atomic positions they can be used to determine whether the crystal structure is ZB or WZ.

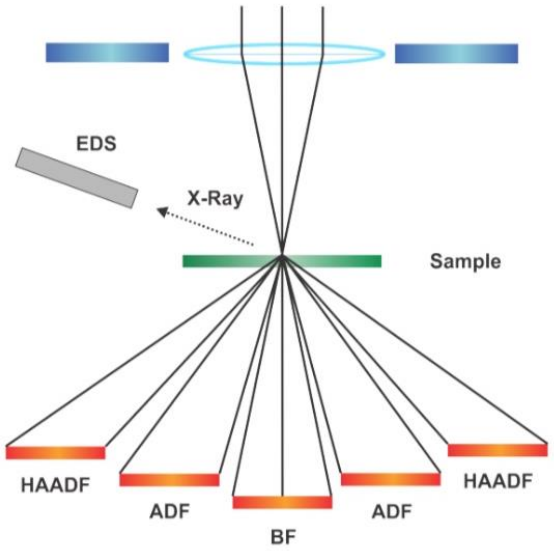

Figure 3.9 – A schematic overview of the different modus available when measuring a sample on the TEM. High-angle annular dark field (HAADF), annular dark field (ADF), bright field (BF) and X-ray diffraction.

In contrast to Bright field images in which the images are generated by a direct beam of electron, it is also possible to generate images from the scattered electrons, known as dark-field images. A schematic of the different angles can be seen in *figure 3.9*. A ring-shaped annular dark field detector is used to measure all the diffracted electrons except the transmitted ones. This has as advantage to see the content of the nanowires, due to its contrast. In this work it is for example possible to see where gold is situated on the nanowire and the branches. High Angle Annular Dark Field (HAADF) images are generated by all the high-angle (>50 mrad) scattered electron collected in the annular dark field detector. The contrast in HAADF images is caused by the atomic number "Z" and the thickness variations in the specimen. Therefore, it possible to study the content of heterostructures. Another way to study heterostructures is by performing Energy dispersive X-ray (EDX) spectroscopy. The electron beam can excite one of the core electrons of the atoms, leaving a vacancy which is then filled by an electron from an outer shell. The energy difference between the two shells is released in the form of an X-ray which is a characteristic quantity for the atomic structure of the chemical element. Which can then be used to image the chemical composition of the heterostructures.

3.4 Experiments performed

In this work research has been done to the growth kinetics of SiGe branches nanowires. To investigate the growth parameters more efficiently, first the temperature was varied between 650°C and 850°C while comparing dislane to tetrasilane and a sample with and without a silicon shell as can be seen in *table 1*. The optimal growth conditions were then later used to further optimize and research the growth kinetics of the Si branched nanowires.

	Si_2H_6 /650°C	Si_4H_{10} /650°C	Si_2H_6 /750°C	Si_2H_6 /850°C
Bare Gap	Sample 1	Sample 2	Sample 3	Sample 4
Sil Shell	Sample 5	Sample 6	Sample 7	Sample 8

Table 1 – A sample overview of the different samples used to investigate the general growth parameters.

To investigate the growth conditions of the Ge branches on Si shell nanowires a temperature series was performed from 320°C to 650°C. Then the Ge content was varied in Si branched nanowires on a Si shell from 21% to 90%. These steps were essential in growing part (2) and (3) of the heterostructure branches, because the growth kinetics are assumable the same as growing branches on a Si shell. By investigating the individual different parts, it could give an insight in the growth mechanics of growing the heterostructure branches as a whole. These heterostructure branches were then finally attempted to be grown.

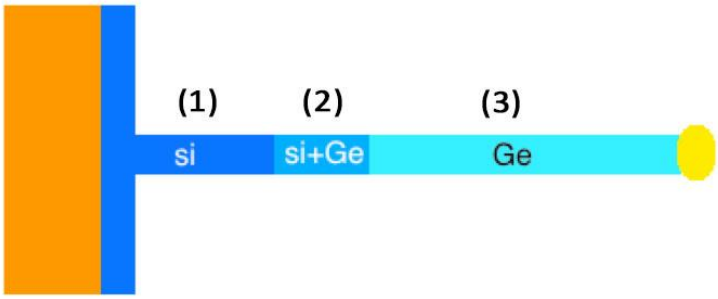

Table 2 – A schematic of a heterostructure branch. A small Si stem (1) is grown on a Si shell GaP nanowire. Then the transition is made from Si to Ge, by incorporating Ge into the branch and terminating the flow of Si precursors (2). When the Si is switched off continuing the Ge branch growth (3).

To investigate the kinking process, the flow of disilane precursor of was investigated from 0.85 sccm to 0.13 sccm, while the growth time was increased to 30 min. to get sufficient long branches to analyze the kinking process. Another temperature series was performed at 0.35 sccm of disilane precursor for 15 min. to investigate the kinking process even further.

4 Results and Discussion

In this work research has been done to the optimization in growing hexagonal SiGe branches and heterostructures. Before getting light emission from the SiGe branches, the branches need to have specific minimal dimensions and the germanium content has to be higher than 65%. For more information see *section 2.2*. To achieve these conditions, first the silicon branches were optimized in terms of precursor and substrate to achieve the widest branches possible in *section 4.2*. Then the optimization concludes in defining the ideal growth regime when varying temperature and flow in which the silicon branches are grown hexagonal (*section 4.3*). The same was done for germanium branches in *section 4.4*.

To study the growth mechanics of the silicon branches in more detail, the kinking of the branches is studied. Theory describes that only parameter affecting the kinking frequency is the flow. Therefore, a flow series is performed. To compare the effect of temperature on kinking a temperature series is also performed in *section 4.5* to study this phenomenon. A detailed analysis of the kinking angle of the silicon branches is done in *section 4.6*. The point of nucleation of the branches is analyzed in *section 4.6* to study the crystal orientation of the branches.

To achieve a germanium content of 65%, germanium was incorporated via the silicon approach in *section 4.7*. Since it was studied how to grow the ideal silicon branches, the ideal germanium branches and how to incorporate germanium into silicon. Heterostructures were tried to be grown in *section 4.8*. These heterostructures include all the key ingredients which are studied in the different optimization steps done in this thesis.

4.1 Optimization of the branches growth

To grow the longest and widest branches, first three different parameters were optimized. This was done while keeping in mind that the crystal structure of the branches has to be hexagonal. The three parameters varied are the type of precursor which are disilane (Si_2H_6) and tetra tetrasilane (Si_4H_{10}), the substrate with and without a silicon shell and two different growth temperatures. When comparing these six samples with one and other it is then possible to say which direction to take to further optimize of the branches growth. This makes it possible to later start incorporating germanium more effectively starting from the Si approach.

4.2 Substrate and precursor

Two different types of precursors were used in this work to see the effects of growing with higher ordered silanes. A higher order silane means that there are more weaker Si-Si bonds present in the precursor compared to the stronger H-Si bonds. This means that the activation energy needed to break the precursors is lowered when moving up in the order of silanes. This gives an activation energy of 2.38 eV and 1.78 eV for disilane and tetrasilane respectively. for more information see *section 2.4.1*. For comparing the two samples the number of Si molecules and growth time are kept the same. Another variable worth investigating is growing Si branches on bare GaP stem or on a Si core-shell nanowire. In theory a defect free Si shell should give better epitaxy, resulting in defect free branches. Since the lattice mismatch between GaP and Si is small both systems could be a potential candidate in growing high quality Si branches. To study the growth kinetics of branches on both systems, four different samples are studied. In *figure 4.1,* four representative SEM images are shown for a sample with a disilane or tetrasilane precursor grown on a Si or bare GaP stem while imaging from the top-view.

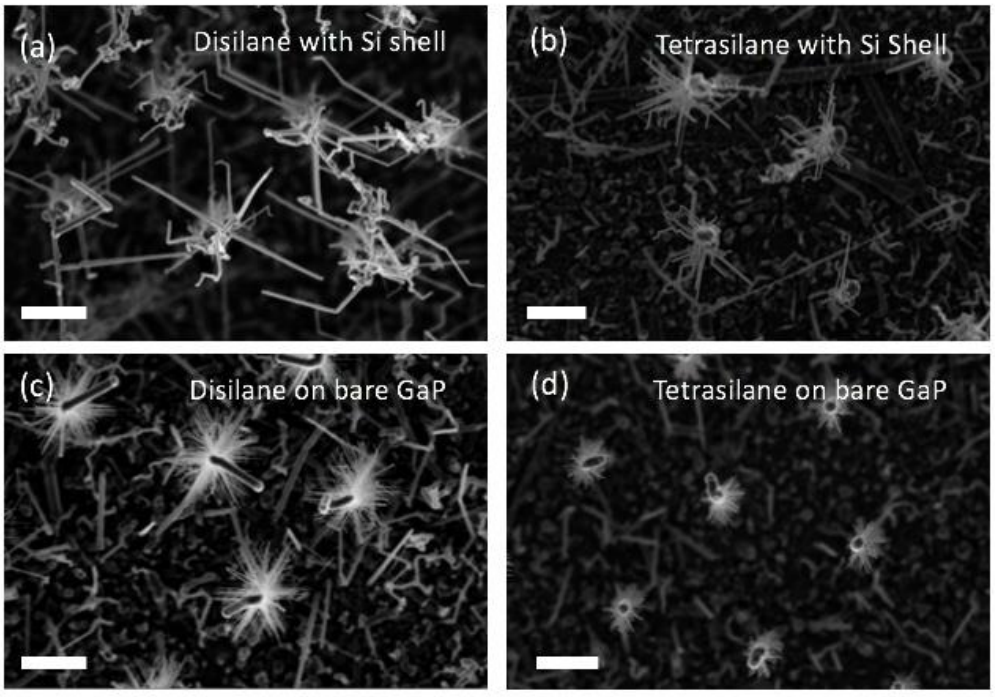

Figure 4.1 - Four representative top view SEM images for silicon branches grown at temperature of 650℃. (a) Disilane grown on a silicon shell. (b) Tetrasilane grown on a Si shell. (c)) Disilane grown on barge GaP. And (d) tetrasilane grown on bare GaP. All the branches are grown for 7min and with a flow of 0.85 sccm. As seen from the images, disilane has longer branches compared to the tetrasilane precursor. The samples including a Si shell shows longer branches compared to the samples grown on

bare GaP. When growing branches on a Si shell, it shows a kinked behavior compared to the samples grown on bare GaP, which do not seem to kink. All the images are taken with a magnification of 25k. The scale bare represents 1µm.

When comparing the precursor disilane to tetrasilane, one can see that the branches are longer for the disilane precursor than the tetrasilane precursor. This contradicts the theory that tetrasilane should grow quicker due to a lower activation energy. Which can then supply more useful precursor material to the gold catalyst. The most important implication is that disilane branches grow the thickest branches on a silicon shell as well as on bare GaP. This can be due to tetrasilane having different growth kinetics at 650°C. The temperature can be too high for tetrasilane resulting in a different breakdown of the precursors. 650°C is the optimized temperature for disilane, but not for tetrasilane.

When comparing branches grown on a Si shell to the branches grown on Bare GaP, one can see that the branches on a Si shell are significantly longer. Also, there is kinking occurring in the system with the Si shell while this is not the case for branches grown on bare GaP. The reason why kinking occurs is to competing growth of other facets, which destabilize the system. Below in *figure 4.2* are two graphs plotted for the thickness measured at the gold droplet and the length of the branches for the four samples.

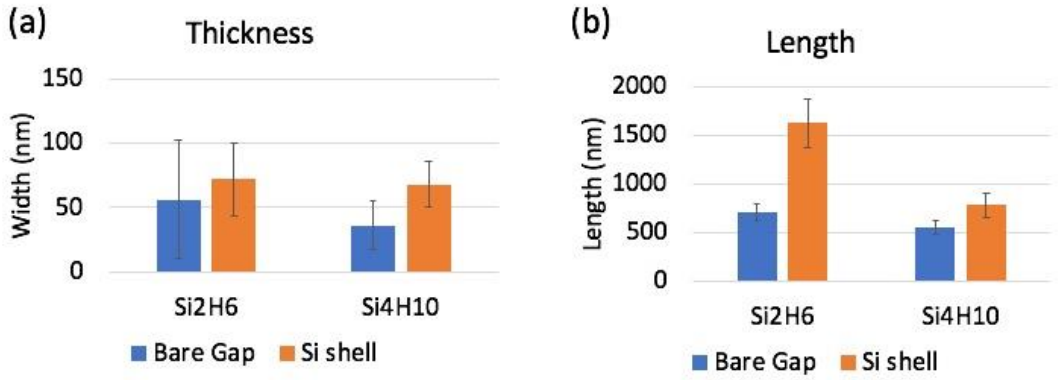

*Figure 4.2 – The width of the branches (a) and the length of the branches (b) for samples with two different precursors grown on bare GaP or on a Si shell. When comparing disilane with tetrasilane, both the width and the length is larger for disilane for different substrates. When comparing branches grown on bare GaP with branches grown on a Si shell, the Si shell shows longer and thicker branches. This is true for both precursors. The width of the branches is measured at the gold droplet interface. The longest branch measured is thus grown by using disilane as a precursor on a Si shell which has a width of 71±2nm and a length of (1,6±0,2)*10^{3}nm.*

Figure 4.2 shows that the longest and widest Si branch is grown by using disilane as a precursor grown on a Si shell. The average dimensions for the branches are 71nm for the width and 1600nm for the length. Since this project is aimed at understanding the growth kinetics of the branches, these conditions were taken as a reference sample for the further optimization of the branches. Also, these conditions were taken for studying the kinking behavior for the branches on a Si shell when varying the flow of precursor.

4.3 Si branches optimization

Using the discovered conditions in the previous section, we further optimized the Si branches by performing a temperature series and a flow series. For both sets of

experiments a as large as possible branch was tried to be grown. The nucleation kinetics and growth rate were studied by performing a time series. To study if the growth rate is linear of and if there is some incubation time present, a time series was performed at a flow of 0.85 SCCM and a temperature of 650°C. The results are shown in *figure 4*.3.

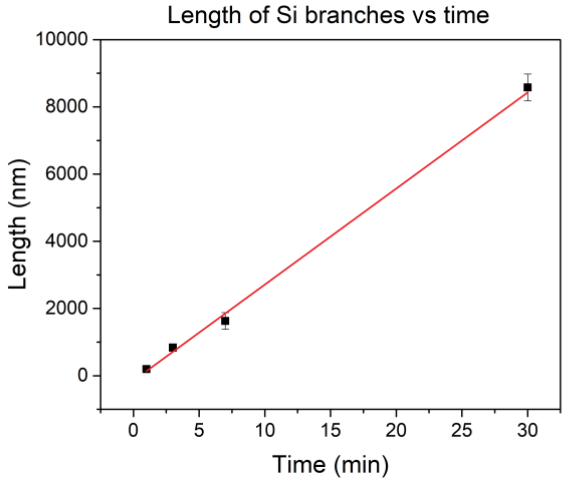

Figure 4.3 – A time series performed at 650℃ in which the length of the branches is measured. All the branches are grown with disilane on a Si shell, with a flow of 0.85 sccm. The growth rate seems to be constant at around 280±10nm per minute. Also, there is no evidence for an incubation time, indicating that the nucleation starts almost immediately after the flow with precursor gasses is opened.

The times series shows that the growth rate is constant and that there is no evidence for a large incubation time. This implies that nucleation starts almost immediately after the precursor gasses are opened. When fitting a linear fit to the data in *figure 4.3*, the length of the branches is around -70nm at time equals zero. This is an indication that the incubation time, if there is any, is around or less than 15 seconds.

4.3.1 Temperature optimization

To study the effect temperature on the growth kinetics of the branches, it was varied at two different molar flows: 0.85 sccm and 0.35 sccm. This was done to find the optimal growth rate and temperature at which the silicon branches are grown thickest. This is important since we want to find the optimal settings to maximize the volume of hexagonal Si material inside the branches. In *figure 4.4* the width and the length of the branches are plotted for different temperatures.

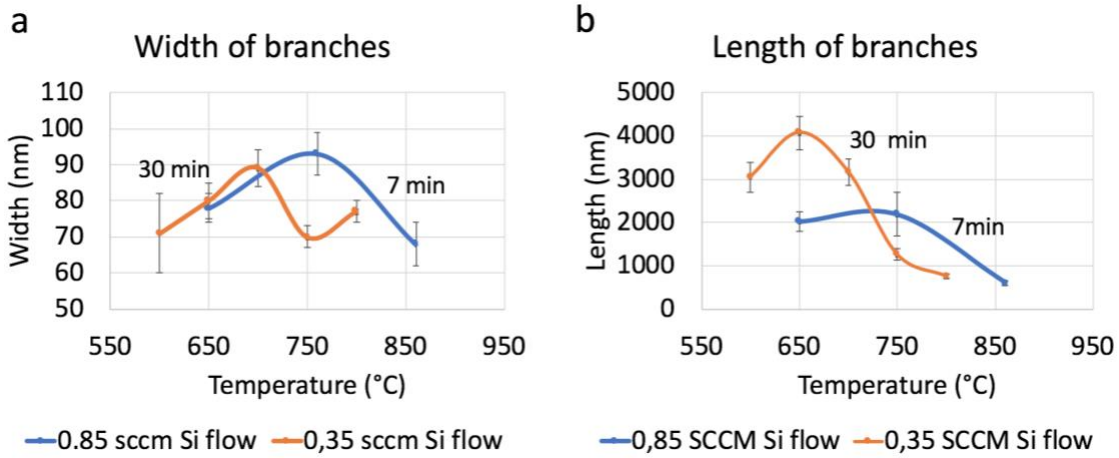

Figure 4.4 – The width of the branches (a) and the length of the branches (b) measured for different temperatures at a flow of 0.35 and 0.85 sccm. The width of the branches is measured at the gold droplet

interface. The samples with a flow of 0.85 sccm are grown for 7 min and the samples with a flow of 0.35 sccm are grown for 30 min. The growth rate is maximized at around 650℃ for 0.35 sccm and is maximized between 650℃-700℃ at a flow of 0.85 sccm. The growth rate is derived considering only the length of the branches. The width of the branches is maximized at 700℃ at a flow of 0.35 sccm and at around 760℃ at a flow of 0.85 sccm. This give an indication that optimal growth regime is between 700-760℃.

The optimal growth conditions are between 700-760°C to grow the thickest branches depending on the flow used. The length of the branches is not of major importance, since the growth time and the length of the branches are linearly related as shown in *figure 4.3*. And thus, longer branches can be grown by increasing the growth time.

4.3.2 Flow optimization

To further optimize the growth regime a flow series was performed to study the effect on the amount of precursor saturating the gold droplet. The flow was varied between 0.13 and 0.85 SCCM. In *figure 4.5* the length and the width are plotted against the molar flow. The width is measured both at the core-shell/branch interface and the gold droplet interface.

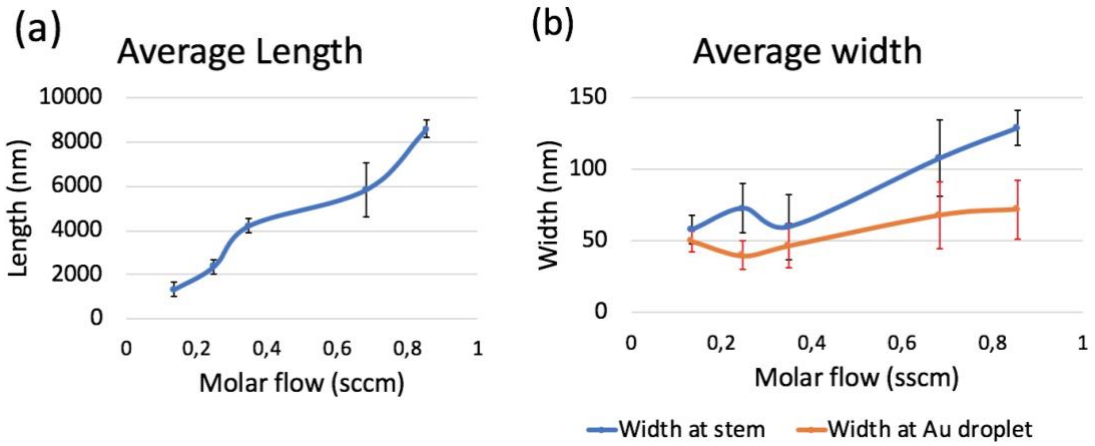

Figure 4.5 - The average length (a) and the average width of the branches (b) when varying the molar flow. The average length is increased when increasing the molar flow. This is due to the amount of precursor material available. The thickness of the branch is also slightly increased when increasing the molar flow. So, a higher flow results in longer and thicker branches.

When increasing the molar flow of disilane, longer and slightly wider branches are grown. This is due to availability of precursors material. The relationship between the flow and the width of the branches is not as evident as the relationship between the temperature and the thickness of the branches. Therefore, one can conclude that temperature plays a more important in the formation size of the gold droplets, than the filling with precursor material does.

4.3.3 Tapering optimization

If the width is measured both at the interface with the stem and at the interface with the gold droplet. The width of the branch seems to be different comparing the bottom with the top of the branch. This phenomenon can be seen when looking at the SEM images when varying the temperature in which a tapering like behavior seems to occur. In *figure 4.6*, three examples of tapering are shown for different temperatures. All the samples are grown with a molar flow of 0.85 sccm for a time of 7 min.

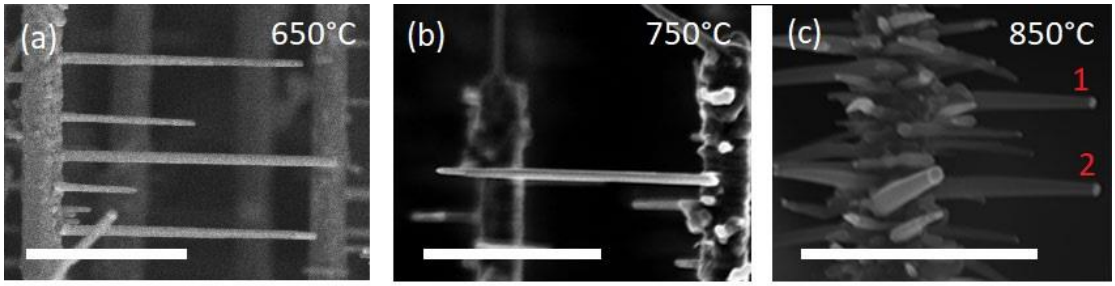

Figure 4.6 – Three different samples grown using disilane on a Si shell with a molar flow of 0.85 sccm for 7min. The temperatures used are 650 ℃ (a), 750 ℃ (b) and 850 ℃ (c). When the temperature increases the tapering seems to increase. Having the most tapered wires at 850 ℃, where (1) and (2) mark two example of tapered wires. The scale bar represents 1µm.

Figure 4.6 shows an increase in tapering when going from a low to a high temperature regime. At 650°C and 750°C the branches are mildly tapered, while they show a predominant tapering behavior at 850°C. Thus, increasing the temperature results into more tapered wires. To proof this concept the tapering rate per micron is calculated. This is the radial width the branch is decreases per micron when moving from the stem to the gold droplet interface. This is done for the branches grown at 0.85 sccm as well as 0.35 sccm.

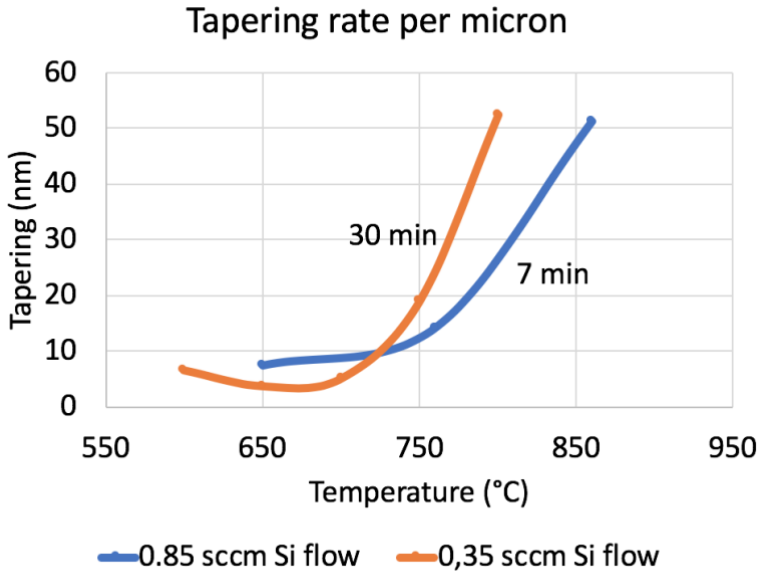

Figure 4.7 – The tapering rate per micron for two different molar flows, 0.85 sccm and 0.35 sccm grown for 7min and 30min respectively. When the temperature increases, the tapering rate increases for both molar flows. This is an indication that radial shell growth is forming since the precursors are cracked more easily at high temperatures in the thin film growth regime.

The tapering rate increases for higher temperatures from around 10nm per micron at 650°C to around 50nm per micron at around 800°C. The reason why the branches become more tapered at higher temperatures is due to the fact that the disilane precursor is cracked more efficiently at higher temperatures without the need of an Au catalyst particle. So, there is film deposition while the Si branch is grown. This can be concluded from the fact that TEM images shows a cubic top (and bottom) facets in the <0001> direction when growing the branches in the <1-100> direction. This is described in more detail in *section 4.3.4.* This means the material is deposited during growth and is not a tapering effect in which the gold droplet shrinks in size during growth.

4.3.4 TEM analysis of Si branches

To check the chemical composition and the crystal quality. A TEM analysis was performed at a sample grown with the disilane precursor with Si shell. The sample was grown for 7 min at 650°C and is shown in *figure 4.8a*. In this sample the branches show a kinking type of behavior and are around 1600nm long and 70nm in diameter. Below in *figure 4.8* the TEM results are shown in terms of crystal quality.

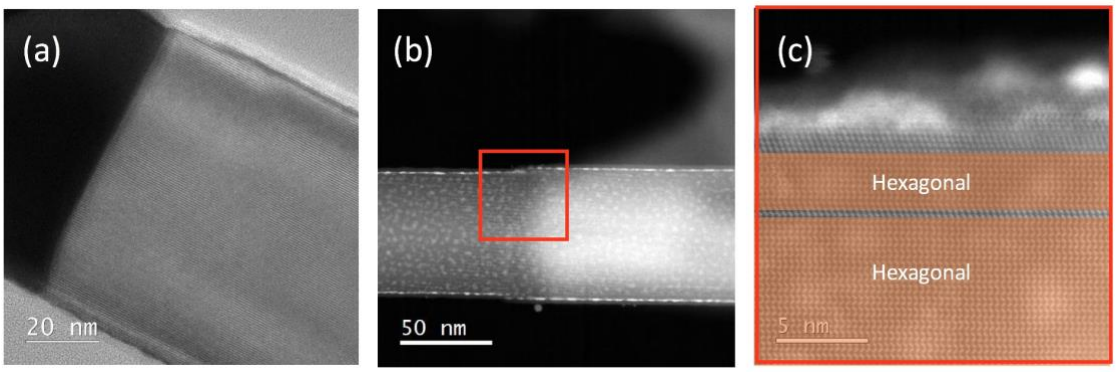

Figure 4.8 – (a) The interface between the branch and the Au catalyst particle. There is no evidence that there is cubic shell growth appearing at the interface. (b) A DF-TEM image from the side of the branch. (c) A HR-TEM image taken from the red box depicted in (b). The hexagonal structure is marked in orange indicating that there is only one stacking fault within the imaged part of the branch. The top facet exhibits a cubic crystal structure. Images (c),(b) is taken in the [11-20] crystal direction.

The HR-TEM image shows that most of the material of the branch is hexagonal except for one stacking fault. This stacking fault is most likely originating from the stacking faults present in the shell. Due to epitaxial copying of the shell, this stacking fault is elongated into the branch. The branch shows cubic top part in the HR-TEM image, which confirms that at the top and bottom facets material is deposited. The branch depicted here has a length of around 1.5μm. With a tapering rate of around 10nm per micron as shown in *figure 4.7*. For a sample with these settings the shell should be around 7 nm thick. This is in the right order of magnitude when considering *figure 4.8a,b*. To see the chemical composition an EDX map was acquired shown in *figure 4.9*.

The EDX map shows the composition of the Si shell and Si branch, in which the Si is the most dominant material. According to the EDX map there is no gold to be present in the Si branches. Another striking feature of the EDX map can be found when comparing the two gold droplets of branch (1) and (2). While the top branch (1) has almost no silicon in the gold droplet, the gold droplet of branch (2) does seem to contain a lot of silicon. This implies that branches can be grown at different saturation levels of silicon. To confirm the absence of gold and to measure the gold droplet composition a more precise chemical composition analysis can be done by using atom probe tomography. Gold is an unwanted material in the branches since it causes deep level traps, which degrades the PL emission. Another contaminant present in the branches is titanium. Titanium is probably present due to contamination within the evaporator and can be removed by running longer coating and stabilization runs before gold deposition.

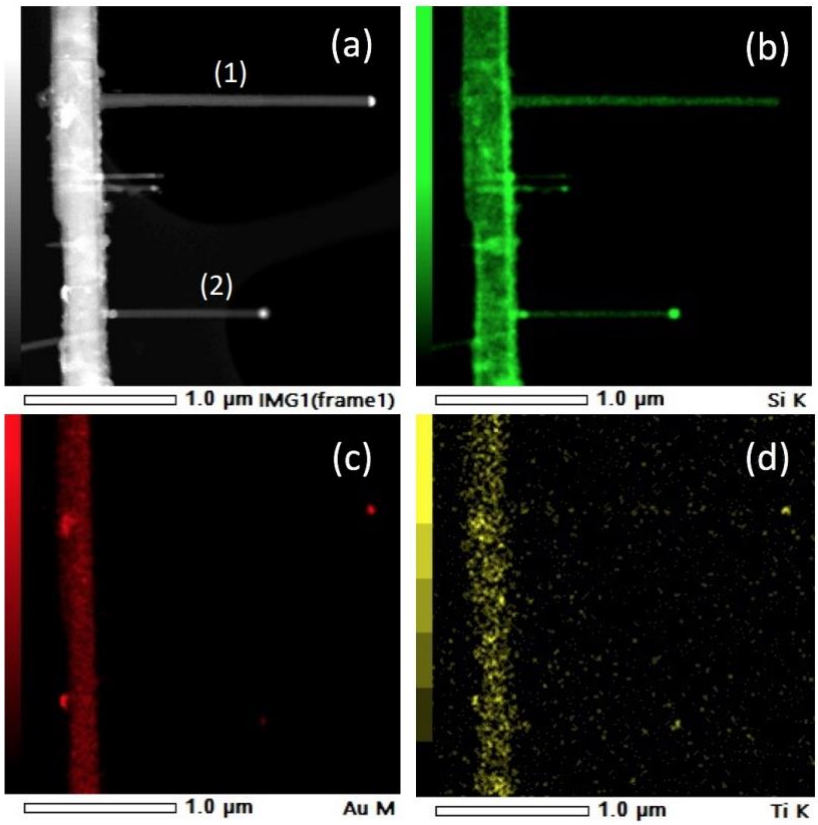

Figure 4.9 – (a) HAADF image of a Si branch on a Si shell. The EDX map shows the amount of Si (b), Au (c) and titanium (d) present in the branch. From (c) one can see that there is almost no gold visible inside the branches. However, there is a lot of titanium found, which is probably due to contamination from the gold evaporator.

To conclude, when growing the longest and thickest branch possible this should be done with disilane was a precursor and on a Si shell. The length of the branch can be made longer by increasing the growth time. The optimal growth rate is around 650-750°C. The thickest branches are grown at a temperature between 700-760°C. The flow plays a minor role in the thickness of the branch but does play an important role for growth rate. A higher flow means that there is more precursor material available and thus the growth rate will increase. For temperatures above 750°C tapering starts to occur which is caused by radial growth on the side facets of the branch. This was also shown in TEM. TEM also showed that the branches are almost entirely hexagonal except from stacking faults originating from the Si shell. And thus, high-quality hexagonal branches can be grown.

4.4 Ge branches optimization

One of the previous members of the group, Håkon Ikaros T. Hauge, has proven that it is possible to grow epitaxial branches on bare GaP cores.[17] In order to merge the optimized branches on Si shell and incorporate more than 65% germanium. It is of great importance to understand the growth regime of Ge branches on a Si shell. Therefore, first a temperature series was performed to optimize the growth temperature regime. Although branches on a GaP core were quite easy to grow, Ge branches on a Si shell resulted in quite a challenge.

To find the right growth temperature many samples were made. Many without success. First a sample at a temperature of 320°C was grown for 3 hours copying the recipe of the successful branches on bare GaP. These branches did not show any form of nucleation, see *figure 4.10a*. Then temperature was increased to 430°C in which no nucleation occurred, as shown in *figure 4.10b*. The small branches on the side walls are an unwanted side effect of an unsuccessful gold etching step before growing the Si shell. When the Si shell is grown these small branches occur due to a little bit of gold residue left overs deposited on the side walls of the nanowire. This can be prevented by flushing longer in water, with the setup described in *section 3.2.4*. The reason why we expect these branches are not germanium branches is because after gold evaporation they leave mask on the substrate in which these branches are visible. This is before growing the Ge branches. Also, the angle of the branches is not horizontal as one would expect after epitaxial growth of the nanowire branches.

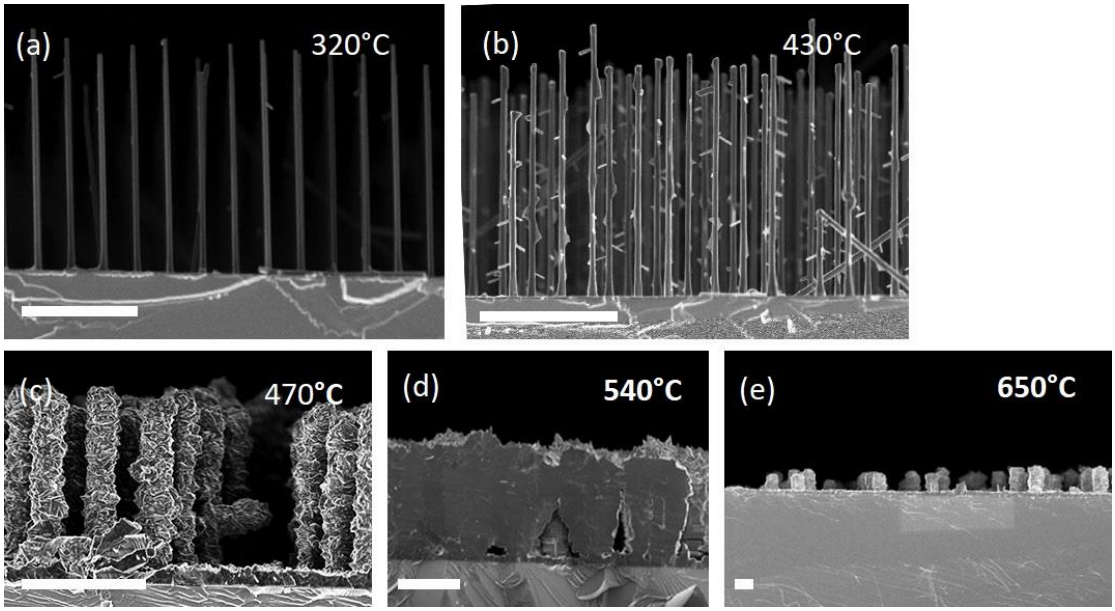

Figure 4.10 – A temperature series Ge branches on Si shell. All the branches are grown of 3 hours with a constant flow of 1.7 sccm. The temperatures used in this series are 320℃ (a), 430℃ (b), 470℃ (c), 540℃ (d) and 650℃ (e). For temperatures of 430℃ and lower no nucleation seems to occur. For temperatures above 470℃ thin film growth starts to occur onto the side facets of the core-shell nanowire. All the scale bars represent 5µm.

When the temperature is increased even further, thin film growth starts to occur for temperatures above 470°C as shown *figure 4.10c*. When the temperature increases the shell becomes thicker eventually coating the entire surface with a layer germanium as

can be seen in *figure 4.10d*. In order to find the right growth regime, the temperature had to be chosen more precisely. The VLS growth regime is expected to be in between the regime of no nucleation and the thin film growth regime. Therefore, a new sample was prepared at a temperature of 450°C, grown for 4.5 hours. The growth time was increase from 3 hours to 4.5 hours, since the incubation time of germanium can be longer than 3 hours and to grow sufficiently long branches so that they can be measured accurately under the SEM. The result when using these setting can be seen in *figure 4.11*, where germanium branches are grown on a Si shell.

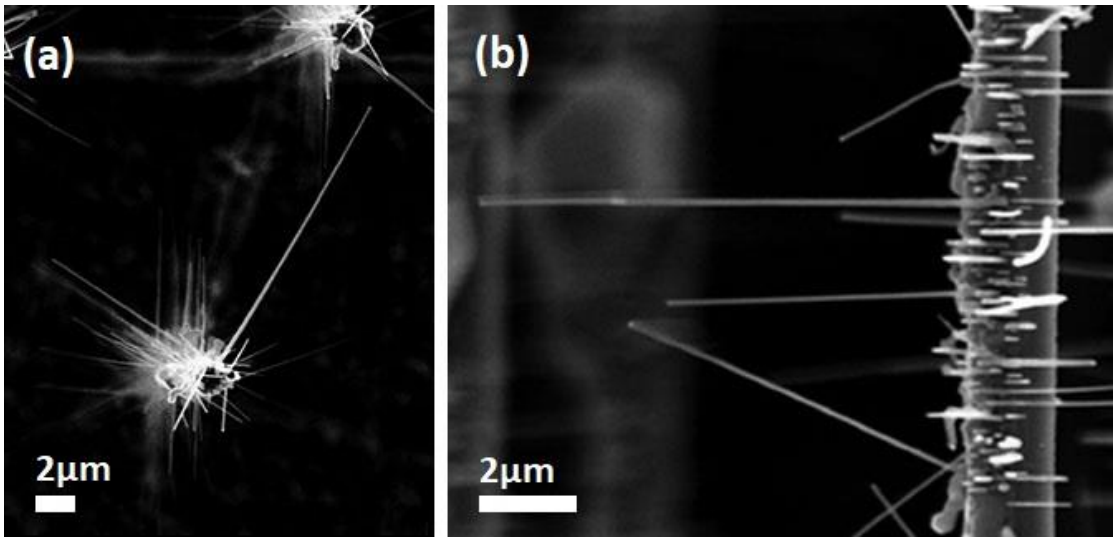

Figure 4.11 – Top (a) and side (b) view SEM image of Ge branches on a Si shell. The branches are grown for 4.5h at 450℃ with a flow of 1.7 sccm. The branches are on average 1340nm long and 11 nm wide.

The average length of the branches are $(1.3\pm0.2)*10^3$nm with a thickness of 10±4nm. These branches are much thinner compared to all the Si branches grown in this work. Also, the temperature regime is much lower than the Si branches, which only nucleate with temperatures higher than 540°C.

4.4.1 TEM analysis of Ge branches

To check the crystal quality and the defects of the Ge branches a TEM analysis was performed on the sample shown in *figure 4.11*. Since the Ge wires are very thin, most of wires have been broken off when transferring the wires from the substrate onto the copper TEM grid. Therefore, only locations very close to the stem of the core-shell nanowire could be imaged. In *figure 4.12* are three TEM images of the Ge branches shown. *Figure 4.12c* shows the crystal structure of the germanium branches which is a mixed phase between cubic and hexagonal germanium.

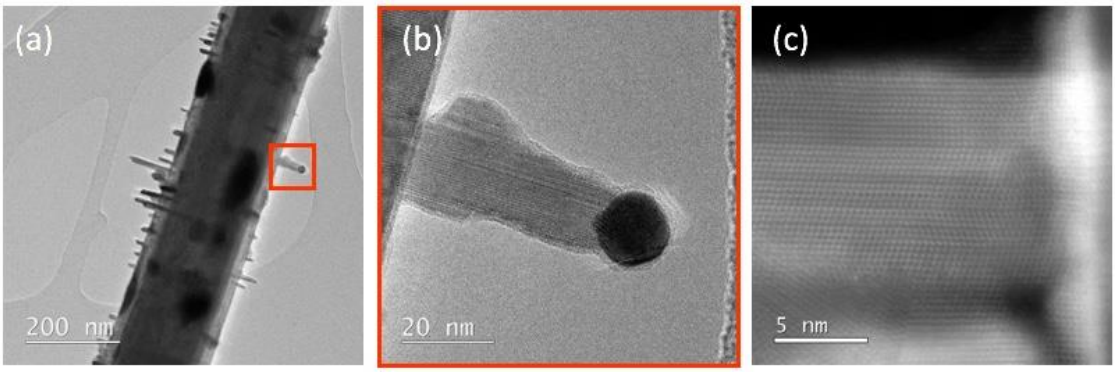

Figure 4.12 – A BF-TEM image of a core-shell nanowire with Ge branches. (a). Most of the nanowires are broken off when transferring to the TEM grid. (b) a zoom-in of the red triangle in (a). A TEM image of a small Ge branch, where the gold droplet is still visible. (c) Is a HR-TEM image of the crystal structure at the interface of the Ge branch and the Si shell interface. The crystal structure is a mixed phase of hexagonal and cubic germanium. Image (c) is taken in the [11-20] zone-axis.

To see the chemical composition of the germanium nanowires, an EDX profile was acquired for Au and Ge shown in *figure 4.13b,c*. When looking at the HAADF image bright white spots are visible on the side walls of the core-shell nanowire. These blobs are an indication of gold, which is confirmed by the EDX map shown in *figure 4.13b*. The EDX map also show that the gold is alloyed with germanium but did not nucleate into a branch.

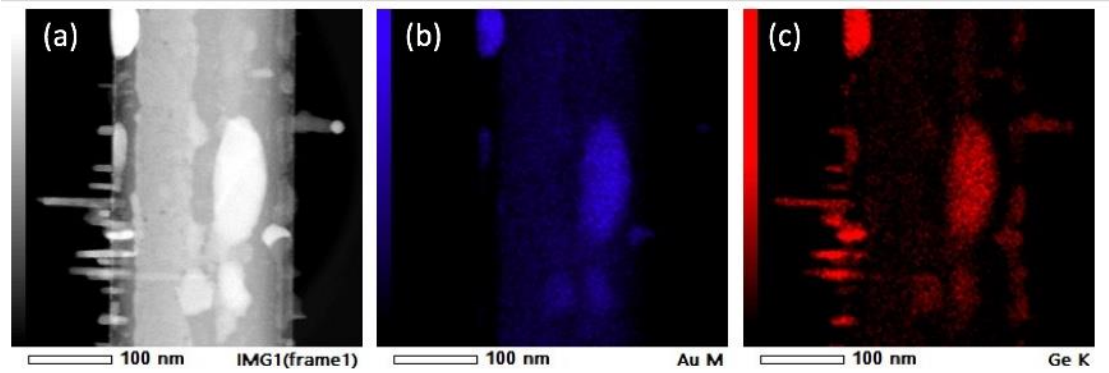

Figure 4.13 – (a) A HAADF image of Ge branches on a Si shell. The white gold droplets on the side ways are an alloy of gold and germanium. This is verified by the EDX map of gold (a) and germanium (b). Images are taken in the [11-20] zone axis.

To conclude, the growth temperature for the VLS growth regime for germanium branches on a Si shell is between 430-470°C. If the temperature is lower, no nucleation will occur. If the temperature is higher thin film growth will be favored over VLS growth. The Ge branches are a mixed phase of a hexagonal and cubic crystal structure, which is unfavorable in this project. The growth temperature regime for germanium compared to silicon branches is off by at least 100°C. This makes it harder to start incorporating Ge into the Si branches and different approached have to be taken to merge the two growth regimes.

4.5 Kinking of nanowire branches

The optimized Si branches grown at 650°C show a lot of kinking, which can be seen in *figure 4.1a.* To get as long and straight nanowires as possible which can be used as gain material in an optical cavity, the kinking has to be minimized. Also, it is interesting to study the kinking behavior in nanowire branches in terms of growth kinetics and if it complies to the theory described in *section 2.5.1* and *section 2.5.2.* According to this theory described on a similar system as the Si branches in this project, the only physical quantity influencing the kinking frequency is the gold particle composition. This gold particle composition can be changed by changing the flow of the precursors which saturate the gold droplet. This changes the contact angle of the gold droplet with the branch interface, making it more or less stable. Therefore, the first experiment performed to proof this principle is changing the flow of disilane precursor to the gold droplet of the branches.

4.5.1 Kinking reduction via flow

To find the optimal stability of the gold droplet the flow was varied between 0.13 sccm and 0.85 sccm. All the branches are grown at 650°C for 30 min. A longer time was used in order to grow branches long enough so that the number of kinks could be counted more accurately when calculating the number of kinks per micron. The number of kinks per micron is calculated by dividing the length of the branch by the number of kinks in that same branch. This is done for the three longest branches per image, for at least 10 images. Below in figure *4.14* are the representative images shown for the different flows used in this series.

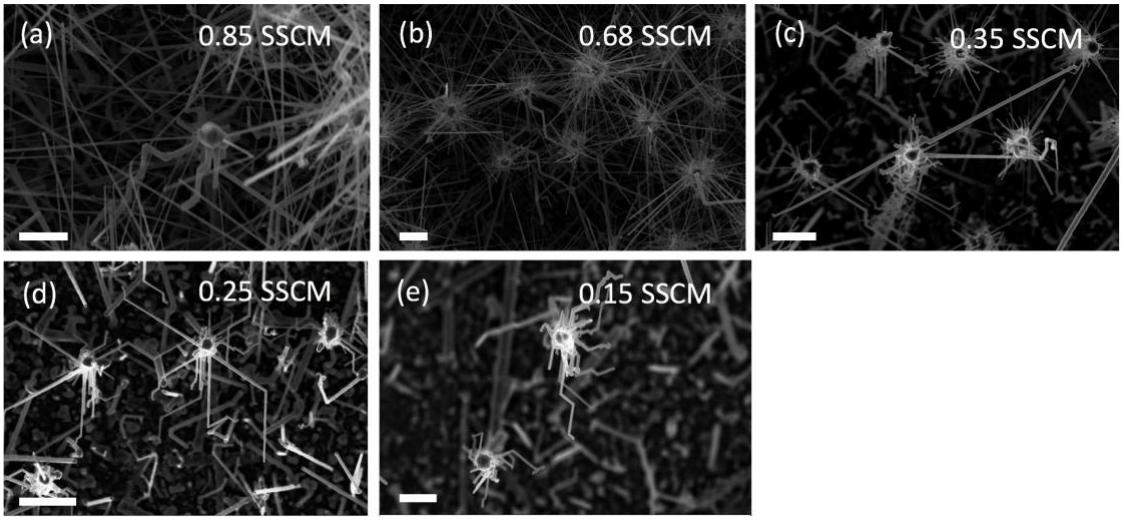

Figure 4.14 – The representative SEM images of the kinking series when varying the flow at 650℃ for 30 min. (a) Show a flow of 0.85 sccm. There is a lot of parasitic growth visible coming from the substrate. Most of the branches seem small, due to the fact they have been broken off. However, longer branches in the order of 9µm can be found which still have a gold droplet. The branches show a heavily kinked behavior. (b) A flow of 0.25 SCCM was used, which shows still a lot of parasitic growth coming from the substrate. The branches show a less kinked behavior. (c) The flow is decreased to 0.35 sccm. No parasitic growth is visible coming from the substrate. The branches are becoming even less kinked, with a higher percentage of the wires being straight. (d) At a flow of 0.25 sccm the wires become more kinked again. (e) At a flow 0.15 sccm the wires become heavily kinked having the shortest average length, with a length around 2µm. All the scale bars represent 1µm.

When starting from the highest flow the number of kinks seems to be decreased when decreasing the molar flow. This is an indication that the stability of the gold droplet

increases when the flow is lowered. When the flow is decreased even further the number of kinks seems to increase. To proof this principle the number of kinks per micron is calculated in *figure 4.15* for the different flows used. Only the branches which are kinked are used to calculate the kinks per micron. Also, the percentage of kinked branches is shown compared to the total amount of branches. Parasitic growth is not included in the statistics.

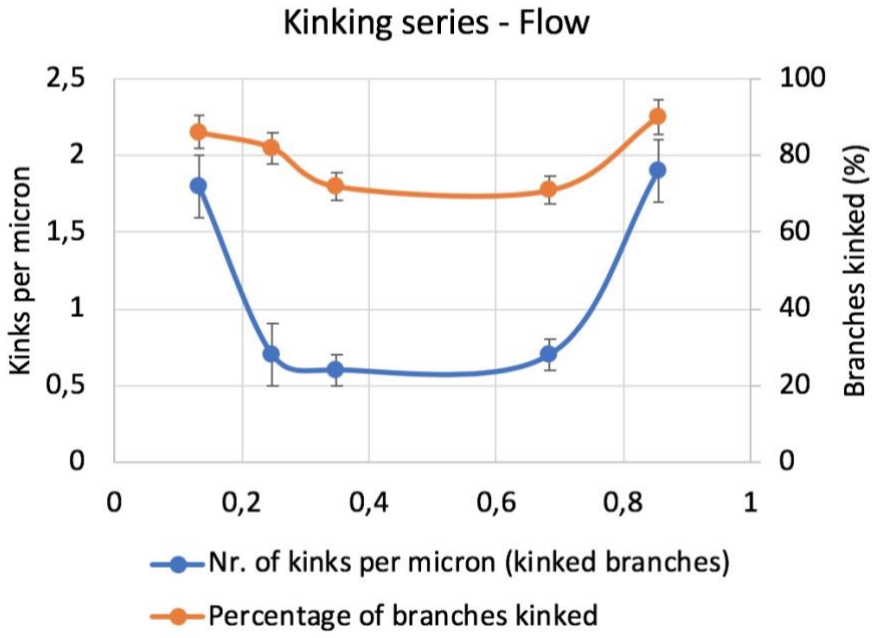

Figure 4.15 – The number of kinks per micron (blue) and the percentage of kinked branches (orange) when varying the flow. The kinking of the branches is least at around 0.35SSCM. The number of kinked branches is minimal between 0.35 sccm and 0.68 sccm.

The kinking is reduced by a factor 3 when the flow is in between 0.25 sccm and 0.68 sccm. This indicates that the stability of the gold droplet is increased in this region, because the gold droplet is not over saturated or undersaturated. Still kinking occurs within the branches. This can be a spontaneous effect of the system which indicates that Si branches on a Si shell will never become a stable system. See more information in theory *section 2.5.1* and *2.5.2*. The kinking percentage was very hard to derive since a lot of wires had to be counted. Although there is a clear dip in the regime between 0.35 sccm and 0.68 sccm, it is hard to make a very accurate estimation of the percentage of wires kinked. To further study the kinking processes a cross-section TEM images was taken in the <11-20> zone axis, shown in figure 4.16. This gives a representation of the cross-sectional shape of the Si branches.

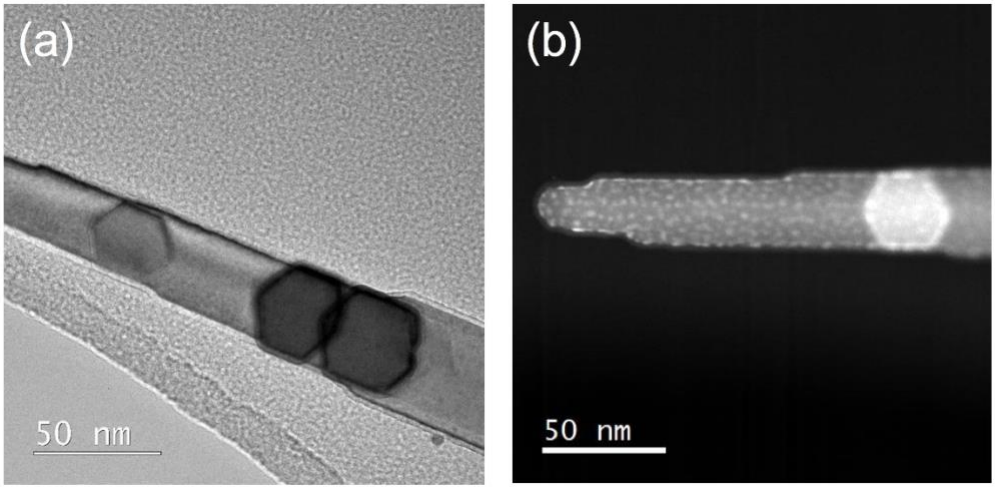

Figure 4.16 – A cross sectional BF-TEM (a) and DF-TEM (b) image of a Si branch on a Si shell. The cross-sectional shape is hexagonal, for all the images taken. The images are taken in the [11-20] direction This is in contrast to the rectangular cross-sections found for Ge branches on a bare GaP, described in section 2.3.5.

The cross-sectional shape is hexagonal for Si branches on a Si shell. This is in contrast to the Ge branches on bare GaP, which exhibit a rectangular cross section. When growing Si branches on Si shell the tapering is around 10nm per micron, which is low compared to samples grown at higher temperatures. Therefore, the cross-sectional shape shown in *figure 4.16* is expected to be the real cross-sectional shape of the Si branches. The cross-sectional shape can be confirmed in later research by performing TEM on a cross-section lamella.

4.5.2 Kinking reduction via temperature

To find out if the sole parameter affecting the gold droplet composition is the flow. A temperature series was performed to see the effect of kinking when the temperature was altered. The temperature was varied between 600°C and 800°C in steps of 50°C. Below in *figure 4.17* are the representative SEM images shown for the different temperatures at a flow 0.35 sccm. At a flow of 0.35 sccm the branches are kinked with a frequency of 0.5 kinks per micron.

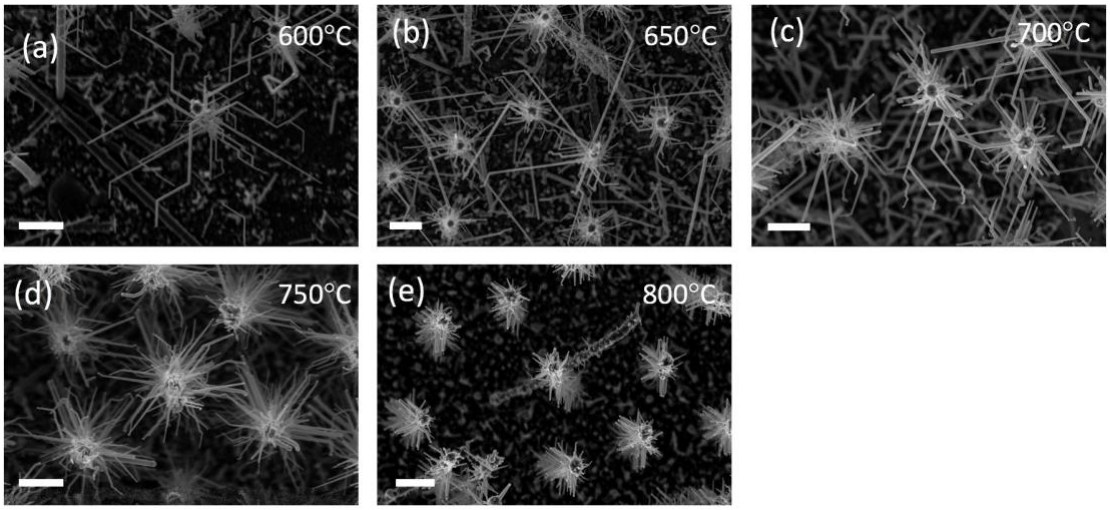

Figure 4.17 – Representative SEM images of a kinking series of Si branches on a Si shell when varying the temperature from 600℃ to 800℃ with a flow of 0.35SSCM for a time of 15 min. In the SEM images of 600℃ (a), 650℃ (b) and 700℃, clear kinking is visible. When the temperature the is increased to

750℃ (d) and 800℃ (e), the branches become shorter, less kinked and more tapered. The tapering is an effect of radial growth which is described in section 4.33. The scale bars represent 1 micron.

When the temperature is increased from 600°C to 700°C the number of kinks per micron seems to be the same. When the temperature is increased to 750°C and 800°C the wires become a lot shorter and the number of kinks reduces, and the tapering increases. The tapering is an effect of radial growth, which is caused by higher temperatures cracking the precursor particles without the need of a catalyst particle. In *figure 4.18* the number of kinks per micron and the percentage of kinked wires is calculated.

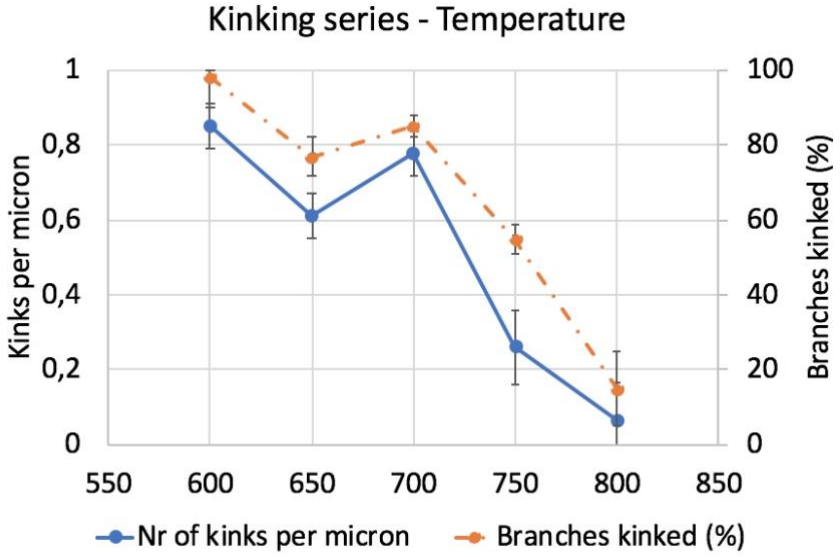

Figure 4.18 - The number of kinks per micron (blue) and the percentage of kinked branches (orange) when varying the temperature. When the temperature increases above 700℃ the number of kinks per micron decreases and also the amount of kinked wires. The percentage of kinked branches is showed with a dotted line, since it was really hard to get a successful estimation and the number might fluctuate on the method chosen.

If the temperature is increased, the number kinks per micron decrease and the wires become shorter. Also, the percentage of kinked branches decreases when the temperature is increased. When comparing the number of kinks per micron in *figure 4.18* to the tapering plotted in *figure 4.7*, the trend is inversed. The number of kinks per micron decreases when the temperature is increased and the tapering rate per micron increases when the temperature is increased. One argument for less kinking occurring in the branches is that the growth rate influences the formation of new layers under the gold droplet. When the new layers form quicker or slower, new facets may arise pushing the gold droplet in another crystal direction. This is makes that a nucleus forms at the active {1-100} facet of the three face boundary, as shown in *figure 2.18*. Another reason can be that solubility of the gold droplet is temperature depended. This changes the composition of the gold droplet which can influence the stability of branches growth.

4.5.3 Kinking angle

The kinking angle is studied by imaging and measuring the wires from the top view in the SEM. According to literature, see *section 2.5.2*, the angle should always be 120°

when a transition is happening from the arm to a triangular joint to an arm in the SBU. In *figure 4.19* are two SEM images shown for the kinking behavior of Si branches on a Si shell. *Figure 4.19a* shows a representative SEM image for the kinking angle for branches and *figure 4.19b* shows an uncommon scenario for kinking angle of Si branches.

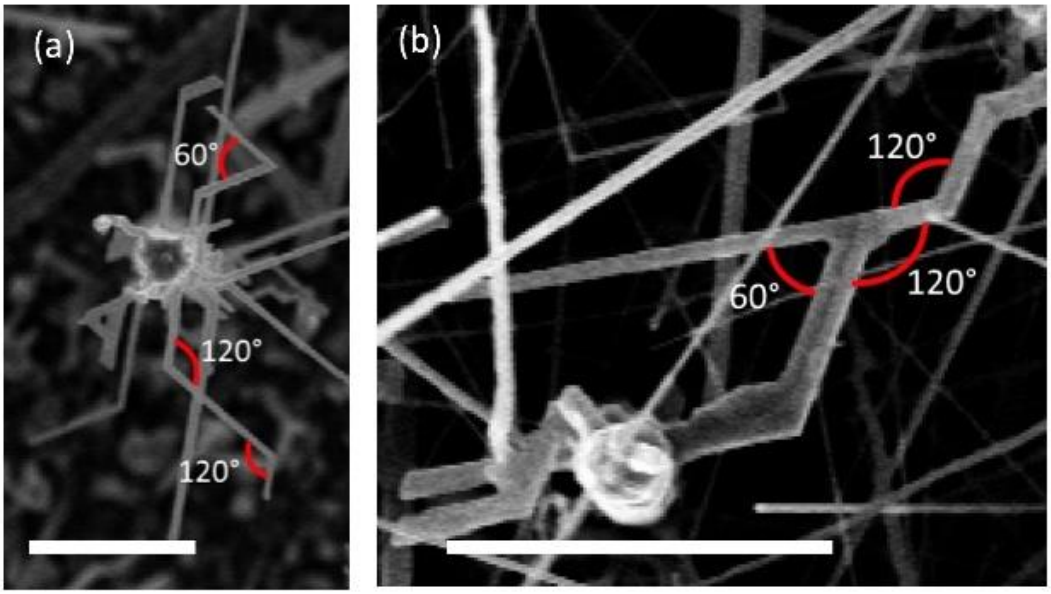

Figure 4.19 – (a) A representative SEM image of the most common kinking angles in branches. These angles are 60° and 120°. The 120° is far more common in the samples. This sample was grown at 650℃, with a flow of 0.15 sccm for 30 min.(b) Represents an uncommon scenario in which the branch splits into two direction. This splitting gives a kinking angle of 60° and 120°. The scale bare represents 1µm.

Most of the branches are kinked at an angle of 120°. This complies with the theory described in *section 2.5.2*, which describes that nucleation happens at the least stable interface. This concludes into growing a triangular joint structure at which nucleation happens again to continue growth in the same crystal direction. By assuming that the interface remains unstable, 60° angles can be grown by growing to connected triangular joints as shown in *figure 2.19a*. This is also observed in other systems found in literature, with a little segment connecting the two triangular joints.[61] The ratio between 120° and 60° depends heavily on the flow used. When the flow is low (0.25 sccm or less), one 60° kink can be found about every ten nanowires on the substrate. This means when taking a SEM picture with 20 nanowires, about 2 nanowires will contain one branch with a 60° angle kink. When the flow is increased, almost no 60° angle kinks are found, and all branches show a 120° angle kink. The 60° angle implies that there is one less stable facet when growing kinked branches from which nucleation is happening from the less stable <11-20> interface, which produces a triangular joint connecting the two arms in the <10-10> direction.

4.6 Point of nucleation

The interface between the core-shell nanowire and the branch is the position where the branch is connected to the stem. During VLS growth the gold droplet becomes super saturated and starts growing in in the preferred crystal direction. To find the crystal direction in which branches are growing, SEM images were taken at a 30° angle. The images show that the branches nucleate at the {11-20} side facet and move over the side facets in the <10-10> direction. The VLS growth continues in the same crystal direction when the side-facet stops. Below in *figure 4.20* are seven images shown which show the point of nucleation at the core-shell interface.

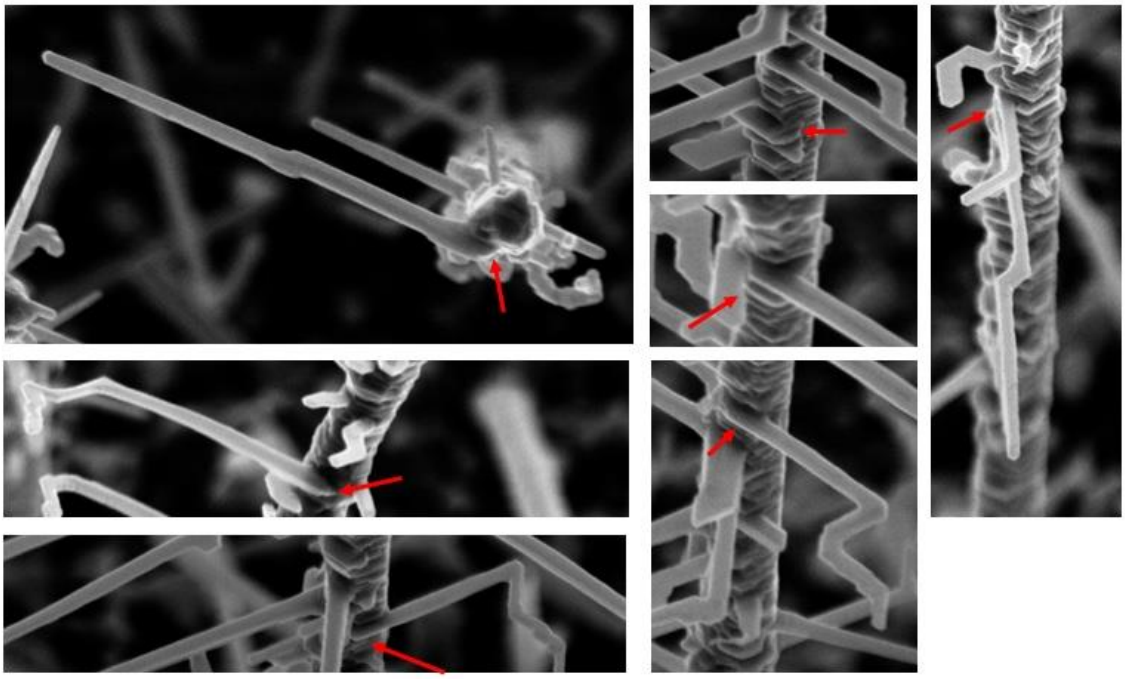

Figure 4.20 – Seven SEM image of Si branches grown on a core-shell nanowire. The red arrows indicate examples of branches following the side facets and continuing in this crystal direction when the side facet stops.

When imaging the point of nucleation in the <11-20> direction with the TEM. The good epitaxial interface between the core-shell stem and the branch is (semi-)flat and the other side away from the interface is hexagonal.

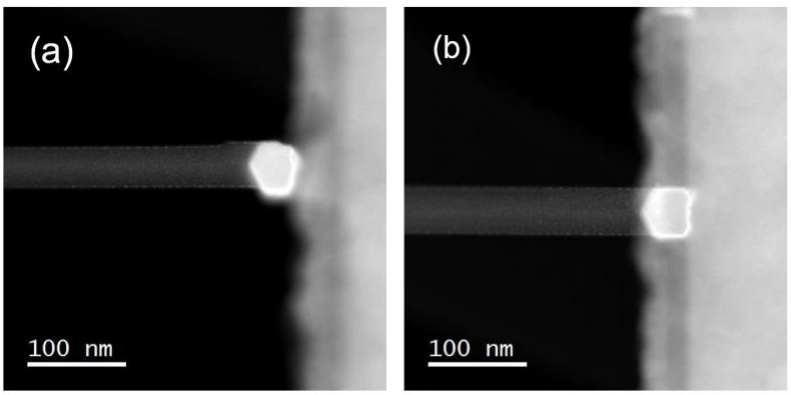

Figure 4.21 – (a) and (b) represent two TEM images of the point of nucleation in the <11-20> zone axis. One side shows a hexagonal facet while the other side has a semi-flat interface with good epitaxy with the core-shell nanowire.

4.7 Ge incorporation via the Si approach

To grow direct bandgap material with an allowed transition. A germanium percentage of 65% or higher in SiGe branches is needed. To study the growth kinetics of incorporating germanium in into a Si branch. The germanium content was increased from 0% to 90%. The branches were grown at 650°C, at a Si flow of 0.25 sccm and for a time of 15 min. In the content series the flow of germanium was tailored to get the right input percentage of germanium, while keeping the silicon flow constant. Consequently, the total flow increases with increasing Ge content. Below in *figure 4.22* are the representative SEM images for the samples with different germanium concentrations.

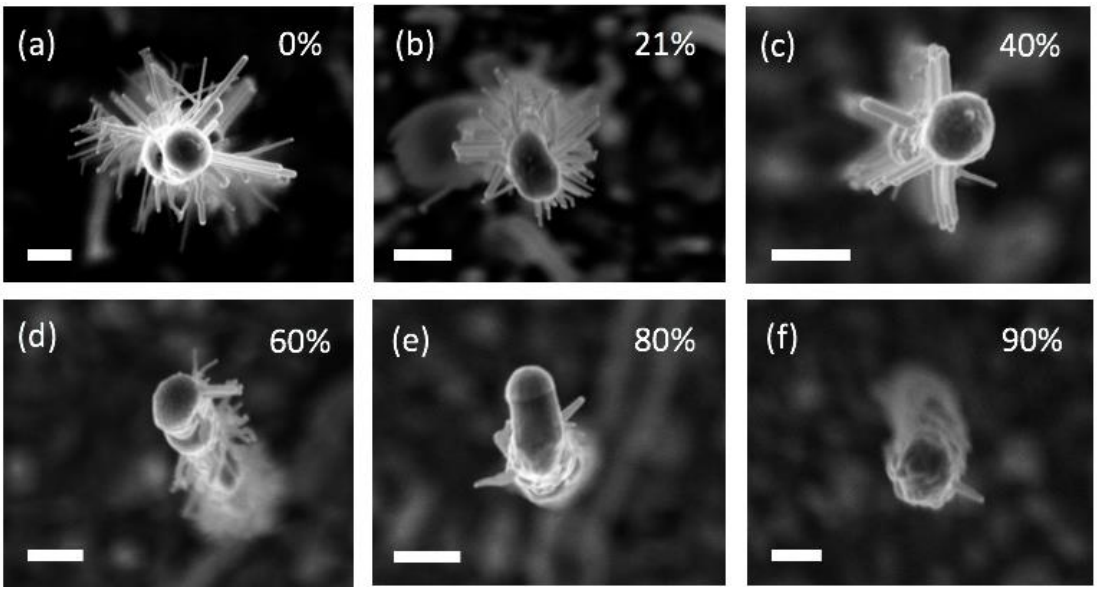

Figure 4.22 – The representative SEM image when increasing the germanium content from 0% (a) to 90% (f). When the germanium content increases the branches become shorter and more tapered. Also, the density of the branches decreases. The scale bar represents 200nm.

With increasing germanium content, the wires become shorter, more tapered and the density of the branches decreases. This can be due to the different growth regimes of the silicon and germanium branches, which grow best at 650°C and 450°C respectively. Above 470°C germanium will be in the thin film regime which implies that only a radial shell will be grown around the core-shell nanowire and the branches. Also, this should imply that the diameter at the gold droplet interface should be constant for all concentrations. Below in *figure 4.23* is the width and the length plotted of the branches.

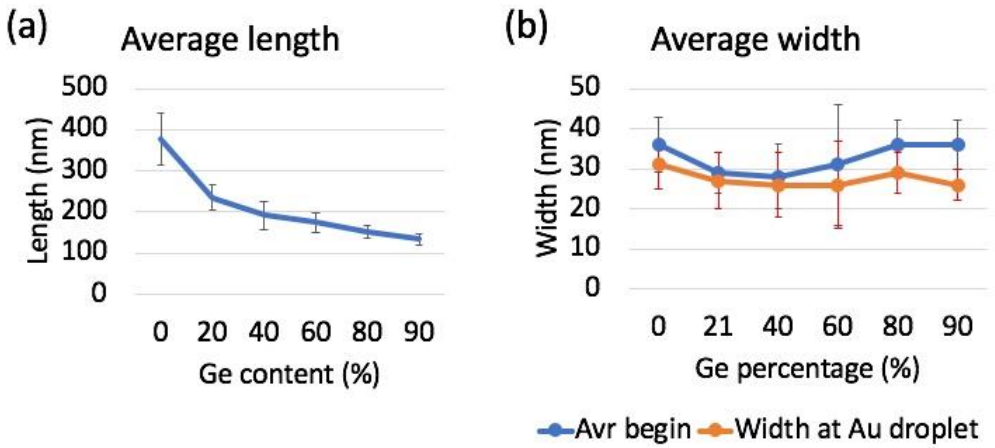

Figure 4.23 – The length (a) and the width (b) of the branches when varying the germanium content in the nanowires. The Length decreases with an increasing germanium content, which is probably due to a high germanium content prohibiting growth in and around the gold catalyst particle. The width of the branches is around the same value of around 30nm for all germanium concentrations.

The average length of the branches decreases with increasing germanium content. However, the width of the branches at the interface between the gold catalyst particle and the branch remains the same. By looking at the tapering rate per micron it is possible to derive whether shell growth is occurring around the branches. The tapering rate per micron is plotted in *figure 2.24*. When the germanium content in the branches increases the tapering increases as well. This indicates that there is a germanium shell growing around the branch. Therefore, the temperature should be lowered when growing SiGe heterostructures, to grow within the VLS growth regime. This might also be the reason that the branches become shorter, since the gold catalyst particle gets buried under a layer of germanium. This prohibits silicon precursor material to reach the gold droplet and therefore there is less nucleation is occurring on the side walls of the core-shell nanowire. When the germanium layer is thick enough, nucleation can come to a halt.

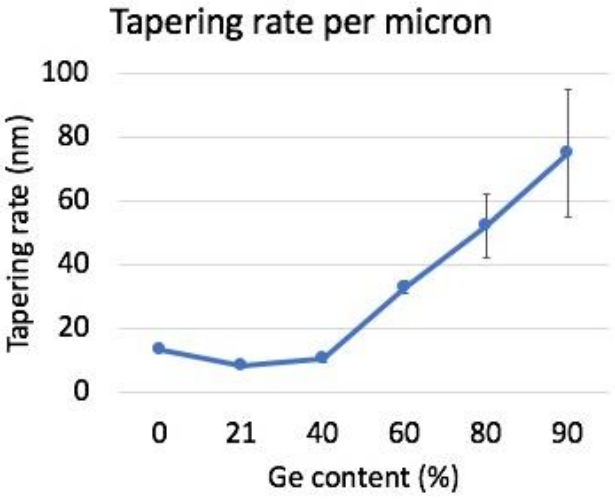

Figure 4.24 – Tapering rate per micron when varying the germanium content in the Si branches grown at 650℃ for 15 min. The tapering rate increases indicating that germanium shell growth is occurring.

4.8 Heterostructures

In this project it was shown that it is possible to grow a 100nm thick hexagonal silicon branches on a silicon shell. It was also shown that it is possible to grow germanium branches on a Si shell. These germanium branches are around 10nm thick and have a mixed crystal structure of hexagonal and cubic germanium. To grow wider germanium branches one approach could be growing a heterostructure as shown below in *figure 4.25*. By growing a small silicon trunk on a Si shell, with a hexagonal crystal structure, this crystal structure can be copied when continuing growth with germanium. By using the silicon trunk as a template, the morphology of the branch allows for the accommodation of strain like in nanowire growth. Since the gold droplet of the silicon branch is larger, this droplet can be used which results hopefully in thicker germanium branches.

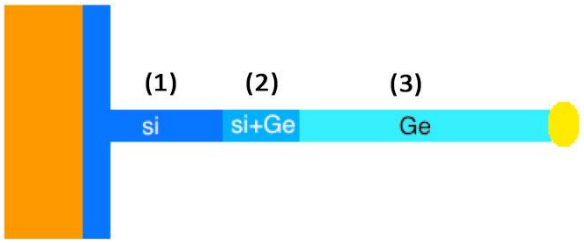

Figure 4.25 – Heterostructures attempted to grow when growing SiGe branches. A small Si branch (1) is grown which acts as a template for the germanium section of the branch (3). The transition made from silicon to germanium is shown in (2).

First a small silicon trunk on a silicon shell was grown at temperature of 650°C, with a flow of 0.85 sccm and a time of 1 minute. The branches are around 200nm long with a diameter of 20nm. An example shown in *figure 4.26a*. When the switch is made by cooling down the reactor to 450°C, lowering the pressure to 25mbar and gradually switching the lines from disilane to germane in 5 minutes. The silicon branches have suddenly disappeared, see *figure 4.26b*. The reason for this is unknown since silicon cannot evaporate via the gold droplet reversibly. Because adsorption is an irreversible process involving dissociation of the source molecule which undergoes a strong exothermic reaction.[62] Also, silicon evaporates at much higher temperature than 650°C. For more information see *section 2.3.1*. To counteract this problem, part (1) of the heterostructure was grown for 3 minutes, making the branches longer. After making the switch (2) to germanium, the branches were still visible under the SEM as shown in *figure 4.26c*.

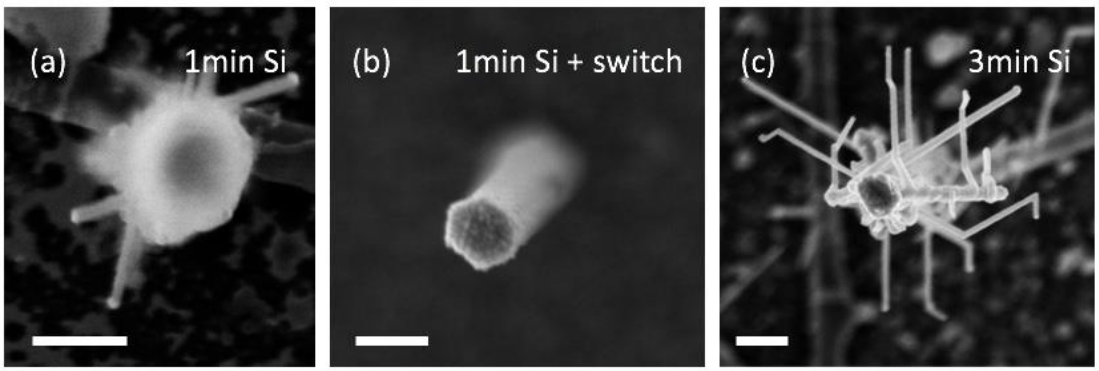

Figure 4.26 – (a) A 200nm long silicon trunk grown for 1 min at 650℃. (b) After making the switch to germanium, the branches have disappeared. (c) The silicon trunk is grown for 3 minutes, resulting in

branches of around 500nm. These branches do not disappear after making the switch. The scale bar represents 200nm.

After making the switch, long SiGe branched heterostructures were tried to be grown. This was tried in several ways. First attempts were made in switching from silicon to germanium simultaneously, while lowering the temperature to 650°C, 450°C and 350°C. This was attempted with varying methods of cooling down: keeping the disilane line open or closing all the lines, varying the reactor pressures at 25mbar or 50mbar, different flows of germanium and different cooling down times. Unfortunately, no visible germanium segments in the SiGe heterostructures were grown. Only at higher temperatures a germanium shell was present around the silicon trunk. This is shown in *figure 4.27*. To grow SiGe heterostructures more research has to be done to the parameters influencing the transition from silicon to germanium. A more precise temperature regime has to be defined and the saturation/filling of the gold droplet with germanium has to be researched.

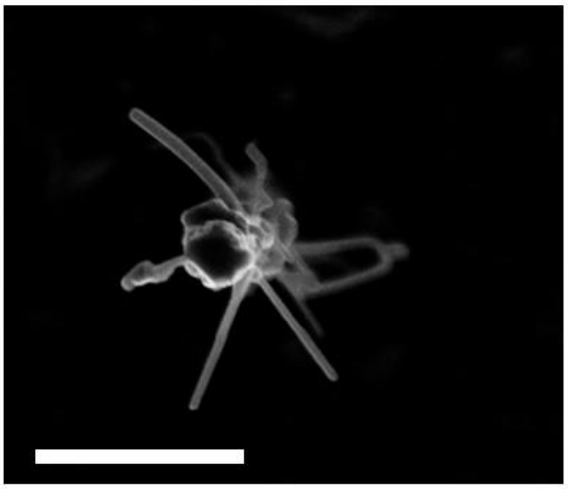

Figure 4.27 – A Si trunk with a Ge shell around the branch. The catalyst gold droplets have almost vanished under a layer of germanium. This sample was grown with 3min of Si at 650℃, a 30 second switch to Ge and Ge branches grown for 5 min at 650℃. The scalebar represents 500nm.

5 Conclusion

To grow the thickest and longest Si branches possible this should be done with disilane as a precursor and on a Si shell. These settings were then used for all later experiments in this report. The length of the branch can be made longer by increasing the growth time. The incubation time is very short and is estimated to be less than 15 seconds. The optimal growth rate has been found for a temperature between 650-750°C. The thickest branches are grown at a temperature between 700-760°C. The flow plays a minor role in the thickness of the branch but does play an important role for growth rate. A higher flow means that there is more precursor material available and thus the growth rate will increase. For temperatures above 750°C tapering starts to occur which is caused by radial growth on the side facets of the branch. This was also shown in TEM analysis. TEM also showed that the branches are almost entirely hexagonal except from stacking faults originating from the Si shell propagating in the branches. And thus, high-quality hexagonal branches can be grown.

To derive the optimal growth regime of germanium branches on a silicon shell a temperature series was performed. The VLS growth regime for germanium branches is between 430-470°C. If the temperature is lower, no nucleation will occur. If the temperature is higher thin film growth will be favored over VLS growth. The Ge branches are a mixed phase of a hexagonal and cubic crystal structure. The growth regime of silicon and germanium branches is off by at least 100°C. Which makes it difficult to merge the two growth regimes for growing direct bandgap material.

To minimize the kinking in the branches a flow and a temperature series were performed. According to literature, the sole parameter affecting the kinking process is the flow which changes the gold particle composition. When varying the flow from 0.15 sccm to 0.85 sccm, a minimum in the number kinks per micron is observed around 0.35 sccm. At 0.35 sccm to 0.68 sccm a minimum is observed in the percentage of kinked branches. This implies that the stability of the gold droplet is greatest at a specific flow, in our case a flow of disilane at 0.35 sccm. TEM images in the <11-20> zone-axis show a hexagonal cross section, which is in contrast to what is earlier described in literature. When increasing the temperature, the number of kinks per micron and the percentage of kinked branches decreases. This could be due to the solubility of the gold droplet being temperature depended and thus changing the gold droplet composition. The kinking angles found are 60° and 120°, which are found in literature for similar structure indicating that there is nucleation happening from the less stable <11-20> interface, which produces a triangular joint connecting the two arms in the <10-10> direction. The number of 60° and 120° angles depends on the flow used. At a higher flow relatively more 60° degree kinks are present on the substrate, indicating that gold droplet is more unstable. The branches nucleate in the <10-10> crystal orientation which was confirmed by TEM.

For a direct bandgap, hexagonal SiGe material is needed with a germanium content higher than 65%. Germanium was incorporated in the branch via the silicon approach. With increasing germanium content, the wires become shorter, more tapered and the density decreases. This is due to the different growth regimes in which the VLS growth temperature for germanium is much lower than silicon. This induces radial growth at high temperatures. At a germanium content above 40%, the gold catalyst particle gets

buried under a layer of germanium. This prohibits silicon precursor material to reach the gold droplet, which decreases the efficiency of nucleation. When the germanium layer is thick enough nucleation can come to a halt. Due to the differences in growth regime between Si and Ge on a silicon shell, no successful heterostructure branches have been grown.

6 Outlook

To create even wider branches other approaches can be investigated. One solution is by thermally lowering the gold droplet which was used for nanowire core growth. This gold droplet is much larger than droplets formed when annealing 10nm of gold deposited on the sidewalls. Probably different growth mechanisms apply for filling the gold droplet compared to branches studied in this work. When lowering the gold droplet thermally, the epitaxial relationship between the sidewall of the stem and the branch should be investigated. Making sure that the crystal quality remains hexagonal. Below in *figure 6.1* is the process shown of thermally lowering the gold droplet to the side wall of the nanowire.

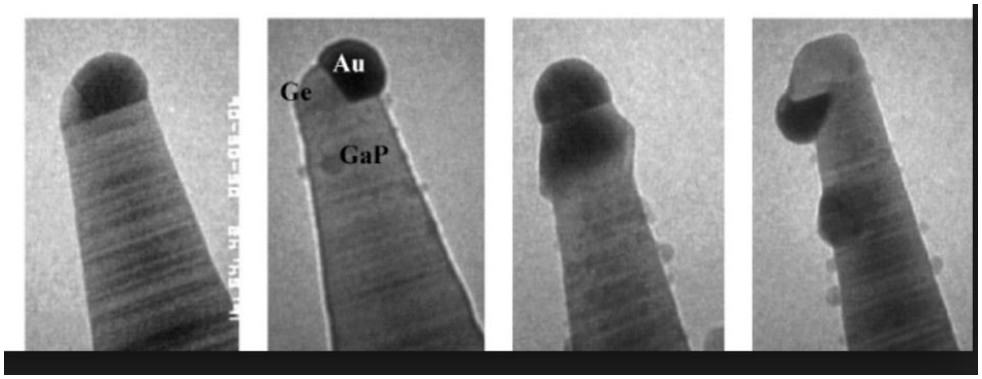

Figure 6.1 – The steps involved in thermally lowering the gold droplet to the sidewall of the GaP nanowire.

Another way to obtain a larger gold droplet size is by using colloids with a diameter larger than the branches grown in this project. Since the diameter size of the gold droplet is of major importance to the width of the branch. Using colloids can be an alternative to gold evaporation. Also the height of the colloids can be tuned by using a polymer layer.[15]

To produce heterostructures on a silicon shell, more research has to be done in merging the growth regimes of silicon and germanium. When switching from silicon to germanium, great caution has to be taken in preventing germanium shell growth. One way to do this could be switching to higher ordered silanes. This lowers the activation energy and thus the growth temperature bringing the growth regimes closer together. One way to produce better $Si_{1-x}Ge_x$ branches might be starting with the germanium approach. Since a germanium content of 65% of higher is required for a direct bandgap, it might be easier to incorporate silicon in germanium branches than visa versa. When starting with the germanium approach it might be easier to use GaAs as a template for the branches, since this Group III-V material is lattice matched to germanium and thus can help to prevent strain.

7 References and Acknowledgements

References

1. Cameron, A. G. W. Abundances of the elements in the solar system. Space Sci. Rev. 15, 121–146 (1973).
2. https://www.waferworld.com/silicon-manufacturing-computer-chips/.
3. https://en.wikipedia.org/wiki/Monocrystalline_silicon.
4. Joannopoulos, J. D. & Cohen, M. L. Electronic Properties of Complex Crystalline and Amorphous phases of Ge and Si. 1. Density of States and Band structures. Physical Review B 7, 2644–2657 (1973).
5. De, A. & Pryor, C. E. Electronic structure and optical properties of Si, Ge and diamond in the lonsdaleite phase. *J. Phys. Condens. Matter* **26,** 1–13 (2014).
6. Kim, T. H. & Lee, J. Y. Hexagonal silicon formation by pulsed laser beam annealing. *Mater. Lett.* **27,** 275–279 (1996).
7. Qiu, Y. *et al.* Epitaxial diamond-hexagonal silicon nano-ribbon growth on (001) silicon. *Sci. Rep.* **5,** 12692 (2015).
8. Bandet, J., Despax, B. & Caumont, M. Vibrational and electronic properties of stabilized wurtzite-like silicon. *J. Phys. D. Appl. Phys.* **35,** 234–239 (2002).
9. Dick, K. A.; Bolinsson, J.; Borg, B. M.; Johansson, J. Nano Lett. 2012, 12, 3200−3206.
10. Larsson,M.W.;Wagner,J.B.;Wallin,M.;Håkansson,P.; Fröberg, L. E.; Samuelson, L.; Wallenberg, L. R. Nanotechnology 2007, 18 (1), 15504.
11. Robinson, R. D.; Sadtler, B.; Demchenko, D. O.; Erdonmez, C. K.; Wang, L. W.; Alivisatos, A. P. Science 2007, 317, 355−358.
12. Hauge, H. I. T. *et al.* Hexagonal Silicon Realized. *Nano Lett.* **15,** 5855–5860 (2015).
13. Joyce, H. J., Wong-Leung, J., Gao, Q., Hoe Tan, H. & Jagadish, C. Phase perfection in zinc blende and wurtzite III- V nanowires using basic growth parameters. *Nano Lett.* **10,** 908–915 (2010).
14. Beaudry, A. L. *et al.* Directed branch growth in aligned nanowire arrays. *Nano Lett.* **14,** 1797–1803 (2014).
15. Dick, K. A. *et al.* Height-controlled nanowire branches on nanotrees using a polymer mask. *Nanotechnology* **18,** (2007).
16. Wang, D., Qian, F., Yang, C., Zhong, Z. & Lieber, C. M. Rational growth of branched and hyperbranched nanowire structures. *Nano Lett.* **4,** 871–874

(2004).

17. Hauge, I. T. Growth of Hexagonal Group-IV Semiconductor Nannowires. (2017).

18. http://www.wikiwand.com/en/Brillouin_zone.

19. Kaewmaraya, T., Vincent, L. & Amato, M. Accurate Estimation of Band Offsets in Group IV Polytype Junctions: A First-Principles Study. *J. Phys. Chem. C* **121,** 5820–5828 (2017).

20. Salehpour, M. R. & Satpathy, S. Comparison of electron bands of hexagonal and cubic diamond. *Phys. Rev. B* **41,** 3048–3052 (1990).

21. Joyce, H. J.; Wong-Leung, J.; Gao, Q.; Tan, H. H.; Jagadish, C. Nano Lett. 2010, 10, 908−915.

22. Kriegner, D. *et al.* Unit cell structure of the wurtzite phase of GaP nanowires: X-ray diffraction studies and density functional theory calculations. *Phys. Rev. B - Condens. Matter Mater. Phys.* **88,** 1–7 (2013).

23. https://www.researchgate.net/profile/Thomas_Vandervelde/publication/236206403/figure/fig2/AS:299382088978435@1448389660391/A-lattice-constant-vs-band-gap-plot-of-common-semiconductor-materials.png.

24. Conesa-Boj, S. *et al.* Cracking the Si shell growth in hexagonal GaP-Si core-shell nanowires. *Nano Lett.* **15,** 2974–2979 (2015).

25. Kittel, C. Introduction to Solid State Physics. (John wiley & Sons, 1971).

26. Zeng, L., Zhao, T. S. & An, L. A high-performance supportless silver nanowire catalyst for anion exchange membrane fuel cells. *J. Mater. Chem. A* **3,** 1410–1416 (2015).

27. Demichel, O. *et al.* Photoluminescence of silicon nanowires obtained by epitaxial chemical vapor deposition. *Phys. E Low-Dimensional Syst. Nanostructures* **41,** 963–965 (2009).

28. https://en.wikipedia.org/wiki/Non-radiative_recombination.

29. Glas, F., Harmand, J. C. & Patriarche, G. Why does wurtzite form in nanowires of III-V zinc blende semiconductors? *Phys. Rev. Lett.* **99,** 3–6 (2007).

30. Lin, J. S., Chen, C. C., Diau, E. W. G. & Liu, T. F. Fabrication and characterization of eutectic gold-silicon (Au-Si) nanowires. *J. Mater. Process. Technol.* **206,** 425–430 (2008).

31. Hall, L. H. The Thermal Decomposition of Germane. *J. Electrochem. Soc.* **119,** 1593 (1972).

32. Donnay, J. D. H. mineralogy. Encycl. Earth Sci. 149–150.

33. Shreck, M., Hörmann, F., Roll, J., Linder, J. K. N. & Stritzker, B. Diamond nucleation on iridium buffer layers and subsequent textured growth: A route for the realization of single-crystal diamond films. Appl. Phys. Lett. 78, 192–194 (2001).

34. Dick, K. A., Deppert, K., Samuelson, L. & Seifert, W. Optimization of Au-assisted InAs nanowires grown by MOVPE. J. Cryst. Growth 297, 326–333 (2006).

35. Lehmann, S., Jacobsson, D., Deppert, K. & Dick, K. A. High crystal quality wurtzite-zinc blende heterostructures in metal-organic vapor phase epitaxy-grown GaAs nanowires. Nano Res. 5.

36. Shtrikman, H. et al. Method for Suppression of Stacking Faults in Wurtzite III−V Nanowires. Nano Lett. 9, 1506–1510 (2009).

37. V. G. Dubrovskii and N. V. Sibirev, Phys. Rev. E 70, 031604 (2004).

38. Algra, R. E. et al. Twinning superlattices in indium phosphide nanowires. Nature 456, 369–372 (2008).

39. E.G. Rochow: The Chemistry of Silicon (Pergamon Press, New York, 1973).

40. Matsumura, M. & Hayama, H. Chemical Vapor Deposition of Amorphous Silicon Using Tetrasilane.

41. Hirose, F., Suemitsu, M. & Miyamoto, N. Surface hydrogen desorption as a rate-limiting process in silane gas-source molecular beam epitaxy. *Jpn. J. Appl. Phys.* **29,** L1881–L1883 (1990).

42. Hazbun, R. *et al.* Silicon epitaxy using tetrasilane at low temperatures in ultra-high vacuum chemical vapor deposition. *J. Cryst. Growth* **444,** 21–27 (2016).

43. Clark, T. E.; Nimmatoori, P.; Lew, K.; Pan, L.; Redwing, J. M.; Dickey, E. C. Nano Lett. 2008, 8 (4), 1246−1252.

44. Fahlvik Svensson, S.; Jeppesen, S.; Thelander, C.; Samuelson, L.; Linke, H.; Dick, K. a. Nanotechnology 2013, 24 (34), 345601. (22) Haapamaki, C. M.; Lapierre, R. R. Nanotechnology 2011, 22 (33), 335602.

45. Paladugu, M.; Zou, J.; Guo, Y. N.; Auchterlonie, G. J.; Joyce, H. J.; Gao, Q.; Tan, H. H.; Jagadish, C.; Kim, Y. Small 2007, 3 (11), 1873−1877.

46. Roper, S. M.; Davis, S. H.; Norris, S. A.; Golovin, A. A.; Voorhees, P. W.; Weiss, M. J. Appl. Phys. 2007, 102 (3), 034304.

47. Hocevar, M.; Immink, G.; Verheijen, M.; Akopian, N.; Zwiller, V.; Kouwenhoven, L.; Bakkers, E. Nat. Commun. 2012, 3, 1266.

48. Zannier, V. *et al.* Nanoparticle Stability in Axial InAs-InP Nanowire Heterostructures with Atomically Sharp Interfaces. *Nano Lett.* **18,** 167–174 (2018).

49. Pan, L., Lew, K.-K., Redwing, J. M. & Dickey, E. C. Stranski–Krastanow growth of germanium on silicon nanowires. Nano Lett. 5, 1081–1085 (2005).

50. Tian, B., Xie, P., Kempa, T. J., Bell, D. C. & Lieber, C. M. Single-crystalline kinked semiconductor nanowire superstructures. *Nat. Nanotechnol.* **4,** 824–829 (2009).

51. Caroff, P. *et al.* Controlled polytypic and twin-plane superlattices in III-V nanowires. *Nat. Nanotechnol.* **4,** 50–55 (2009).

52. Algra, R. E. *et al.* Twinning superlattices in indium phosphide nanowires. *Nature* **456,** 369–372 (2008).

53. Lugstein, A. *et al.* Pressure-Induced Orientation Control of the Growth of Epitaxial Silicon Nanowires. *Nano Lett.* **8,** 2310–2314 (2008).

54. Qian, F. *et al.* Gallium nitride-based nanowire radial heterostructures for nanophotonics. *Nano Lett.* **4,** 1975–1979 (2004).

55. M. A. Verschuuren and S.F. Wuister, 'imprint lithography,' 2008.

56. Assali, S. Pure crystal pahse nanowires: growth and optical propterties. (2015).

57. G. Stringfellow, Organometallic Vapor-Phase epitaxy: theory and practice. second ed., 1999.

58. Jones, A. C. & Hitchman, M. L. Overview of Chemical Vapour Deposition. (2009).

59. M. T. Borgström, J. Wallentin, J. Trägardh, P. Ramvall, M. Ek, L. R. Wallenberg, L. Samuelson, and K. Deppert, "In situ etching for total control over axial and radial nanowire growth," Nano Research, vol. 3, pp. 264–270, Mar. 2010.

60. Investigation of multiferroic and photocatalytic properties of Li doped BiFeO3 nanoparticles prepared by ultrasonication - Scientific Figure on ResearchGate. Available from: https://www.researchgate.net/Schematic-diagram-of-Field-Emission-Scanning-Electro.

61. Lieber, C. M. NIH Public Access. **36,** 1052–1063 (2012).

62. Kodambaka, S., Tersoff, J., Reuter, M. C. & Ross, F. M. Diameter-independent kinetics in the vapor-liquid-solid growth of Si nanowires. *Phys. Rev. Lett.* **96,** 1–4 (2006).

Acknowledgments

I would like to thank a few persons for their guidance and help with this research project. First of all, Msc. Yizhen Ren, my daily supervisor. Thanks for the willingness to help during the experiments, during data analysis for presentations during the group IV meetings and the guidance throughout the year. Special thanks to prof. dr. Erik Bakkers for the overall supervision and giving me the opportunity to work at his group. I would also like to thank dr. Marcel Verheijen for the TEM-analysis and for his interest in this project by sending papers with useful information. I also thank the technicians in the cleanroom, especially Rene, Frank and Barry who have helped me a lot during experiments. And of course, thanks to other PHD students, postdocs and staff members of the AND group who have helped me during the scope of this project. Thanks to Silas and Microsoft funding this project. Finally, I would like to thank my family, father, girlfriend and friends for supporting me inside and outside my academic career.